Study of neutral π meson in $\sqrt{s_{\mathrm{NN}}} = 5.02$ TeV p+Pb collisions with the PHOS detector at ALICE

(核子対あたり重心系衝突エネルギー 5.02TeV の陽子+鉛原子核衝突における
ALICE 実験 PHOS 検出器を用いた中性 π 中間子の研究)

Tsubasa Okubo

M124765

Experimental Quark Physics Laboratory
Department of Physical Science
Graduate School of Science, Hiroshima University

Supervisor : Prof. Toru Sugitate
Primary examiner : Prof. Toru Sugitate
Examiner : Prof. Yasushi Fukazawa

February 28, 2014

Abstract

Quark-gluon plasma(QGP) which is believed to have existed in a very early universe, is a high temperature and energy density matter. The ALICE experiment specializes in heavy-ion collisions and is intended to explore the property of QGP. It is thought that elucidation for the property of QGP leads to explore the origin of matter and the state of very early universe. The hadron yield suppression is one of results for indicating generation of QGP. The yield suppression for π^0 meson is interesting because π^0 meson is the lightest in all hadrons.

The PHOton Spectrometer(PHOS) is a electro-magnetic calorimeter to observe QGP at the ALICE experiment. PHOS consists of a lead tungsten (PWO) which is inorganic scintillator crystal and avalanche photo-diode (APD) read out. It has a wide dynamic range, excellent energy resolution and high granularity. These advantage enables photon measurement of high precision.

In this thesis, we analyzed minimum-bias triggered data measured by PHOS in p-Pb collisions at $\sqrt{s_{\mathrm{NN}}} = 5.02$ TeV. First we judged and sorted the stability of constitution cells and period when PHOS works normally based on measured energy and detected particle number. This is essential part in analysis so as to attain the reliable results. After that, we measured energy-to-momentum ratio for electron to investigate the accuracy of energy measurement in PHOS. The energy of electrons was measured by PHOS and their momentum was measured by charged particle track detector(TPC). A particularly conspicuous non-linearity effect at low p_{T} region was evaluated. Then the invariant mass was reconstructed from detected photon pairs. We measured π^0 meson raw yield by extraction of signal peak from the invariant mass distribution. In addition, the geometrical acceptance of PHOS and reconstruction efficiency for π^0 meson were estimated with Monte Carlo simulation. We discuss about efficiency corrected π^0 yield.

Contents

List of Figures

List of Tables

1 Introduction

1.1 Standard model

For a number of years, a searching the elementary particle that is minimum particle constructing matters, has been studied. The atom, which means minimum element constructing matters and impossibility to separate it, was found out in 19th centuries. At that time, it was believed all matters are composed from atoms and the atom is elementary particle. However because atoms have hundred or more different types and cyclical nature, we thought they have inner structure. It was found the atom consists of nucleon and electrons circling around the nucleus, and the nucleus consists of protons and neutrons after investigation. Recent studies show protons and neutrons are composed of quarks. In present, we believe that quark and lepton are elementary particle and study fine structure based on standard model. Baryon such as proton and neutron consists of three quarks and meson such as pion consists of quark and anti-quark pair. The quark and lepton have each 6 different types. The quark contains up, down, charm, strange, top and bottom and the lepton contains electron, muon, tau particle and neutrinos corresponding to each particle. They are categorized as three generation (Figure 1).

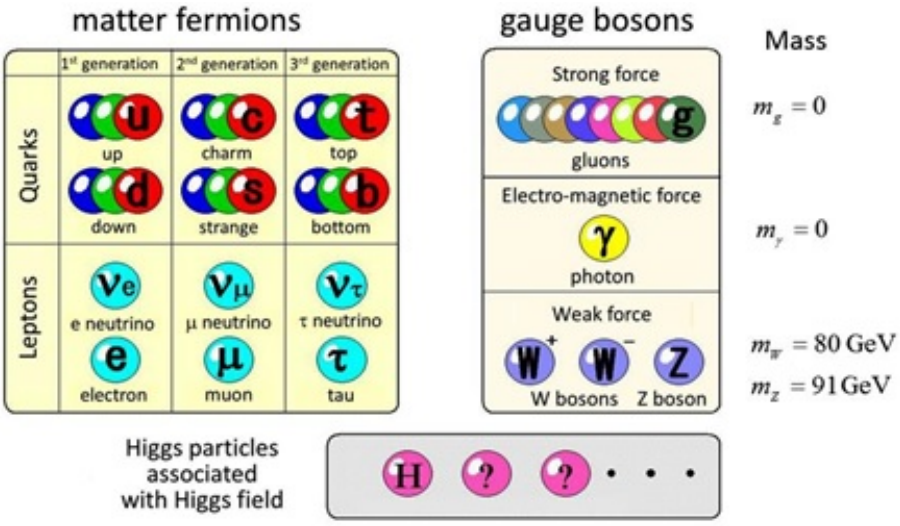

Figure 1: Standard model

According to the standard model, forces interact between these elementary particles. They are strong interaction, weak interaction, electro-magnetic interaction and gravity. These forces interact by the medium of particle called gauge boson. We can feel effects of electro-magnetic interaction and gravity, but we cannot feel the effects of strong interaction and weak interaction because they affect only in ultra-microscopic space like a inside of nucleus. The gravity operates on every matter having mass. It is believed the gauge boson is graviton, but the particle still has not found. The severity of force is proportional to the mass and inversely proportional to the squares of distance. The gravity is very small force but it can make a bound system such the universe because the reachable distance is

so long. The electro-magnetic interaction operates between charged particle and the gauge boson is photon. The electro-magnetic force can reach infinity distance and severity of the force is proportional to charge amount and inversely proportional to the squares of distance. The weak interaction operates between all quarks and leptons. The gauge boson is weak boson and it includes W boson which has charge and Z boson which does not charge. This interaction is called "weak" because it is very small inside of the nucleus. The strong interaction dominates in inside of the nucleus and operates between quarks which have color charge. The gauge boson is gluon. Mesons consist of quark and anti-quark but it is difficult to separate them. Because they are connected by the force to be strongly bound than more you try to separate them. Even if we were able to separate them, quark and anti-quark pair are produced between them. Then separated quark combines with new quark and new meson is produced. It can not be taken out quark by itself due to this property. It is called "quark confinement".

interaction	strong	weak	electro-magnetic	gravity
origin	color charge	weak isospin	charge	mass
coupling constant	~ 1	10^{-5}	$1/137$	10^{-39}
distance[m]	10^{-15}	10^{-17}	∞	∞
medium particle	gluon	weak boson	photon	(graviton)

Table 1: Four interactions and the property

1.2 Quark Gluon Plasma

The big bang theory says the universe was created about 137 hundred million years ago by the big bang and expanded rapidly (called inflation). It had been state of high temperature and energy density in early time on the creation of the universe after the inflation. Then, quark pair, gluon, photon and lepton were generated and the universe at present was formed in this manner. In this high temperature and energy density state, quark and gluon could move about freely and the state is called Quark-Gluon Plasma(QGP). The QGP diagram is shown in Figure 2. It is important to study of the matter state on high temperature and energy density in early time on the creation of the universe in order to understand evolutional process of the universe.

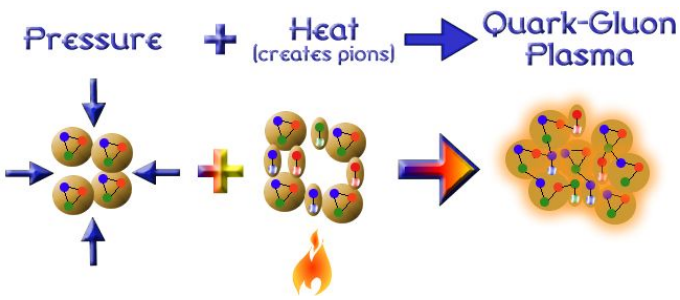

Figure 2: QGP diagram

We believe quark and gluon are elementary particle, but we can't take out them independently

according to the Quantum Chromo-Dynamics(QCD). It is impossible to generate QGP in common temperature and energy density due to the property of quark confinement. The way of break confinement is achieving high temperature and/or high energy density. The high energy heavy-ion collisions experiment is only way to be able to generate QGP by artificial means.

The lattice QCD calculations predict that the phase transition to the QGP state occurs at a critical temperature, T_c, of 150-200 MeV. Figure 3 shows the calculated results of the entropy density s/T^3 as a function of temperature T[1]. The entropy density increases stepwise the deconfinement of the matter.

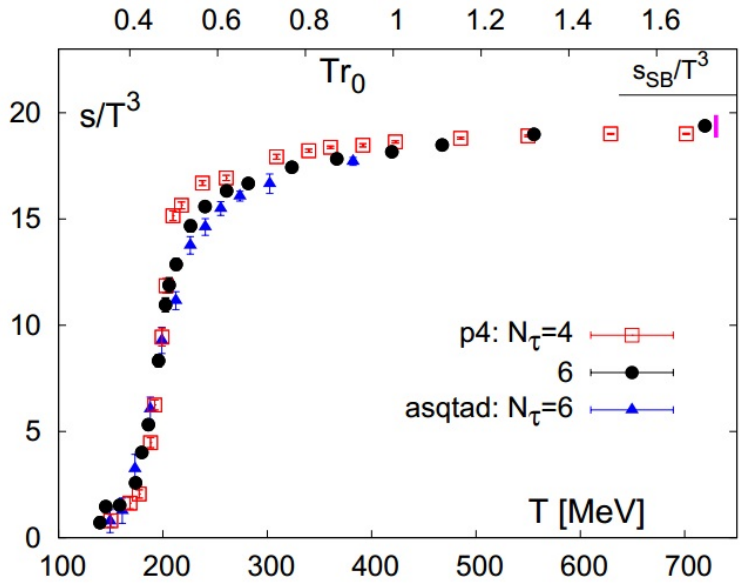

Figure 3: Theoretical calculation based on lattice QCD

A schematic phase diagram of hadronic matter including QGP is shown in Figure 4. The horizontal axis is the baryon density normalized to the density of the normal nuclear matter ($\sim$0.15 GeV/fm^3) and the vertical axis is the temperature. QGP is considered to have existed in high temperature circumstances of the early universe, a few micro second after the Big Bang.

1.3 High energy heavy-ion collisions

We explain about time evolution for high energy heavy-ion collisions (Figure 5) in this section.

1. The nuclei accelerated close to the speed of light become disk-shaped such as pancake by the Lorentz contraction. They collide with each other.

2. The colliding nuclei sneak through each other because they have very high energy. Then the space after sneaking through has a high temperature and energy density. The structure of nucleon is lost in the very early stage of reaction and quark and gluon released from the nucleon

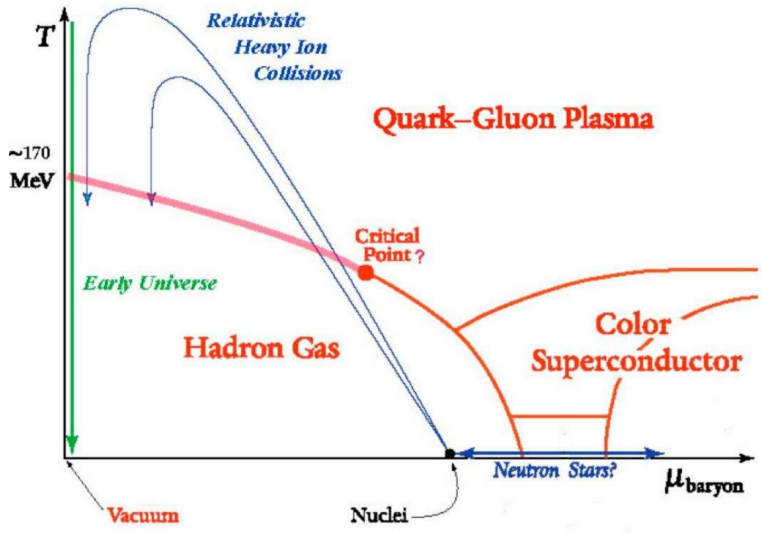

Figure 4: A schematic phase diagram of QCD matter

repeat scattering. The spectator which is part not participated in the reaction, proceeds leave the speed of light.

3. The reaction region is left behind and a lot of quark, anti-quark and gluon are generated in this region. When this high density state has sufficiently-long duration, high temperature state reached thermal equilibrium is generated. The state is called QGP.

4. The QGP expands with speed close to the speed of light by high pressure from the internal and the temperature of QGP drops. After that quark and gluon recombine. It generates hadron gas state after passing through the intermediate state coexisting deconfinement phase of quark and hadron phase. Eventually, generation of particles can be eliminated and number ratio of particles is fixed (called chemical freeze-out).

5. Further energy density decreases by expanding and it doesn't do the elastic scattering of hadron each other (called thermal freeze-out). After freeze-out, all particles defuse.

We can measure only the sum of all particles after having passed through the above process.

1.4 Photon measurement

A huge number of charged and neutral hadrons, leptons and photons are produced in high energy nucleus collisions. In various particles, photon measurement is one of the important because photons in high transverse momentum(p_{T}), called prompt photon, prevail for validation of perturbative QCD(pQCD), and photons in low p_{T}, called thermal photon, become a probe to convey information of initial state for QCD matter such as QGP. The advantages of photon measurement are directed

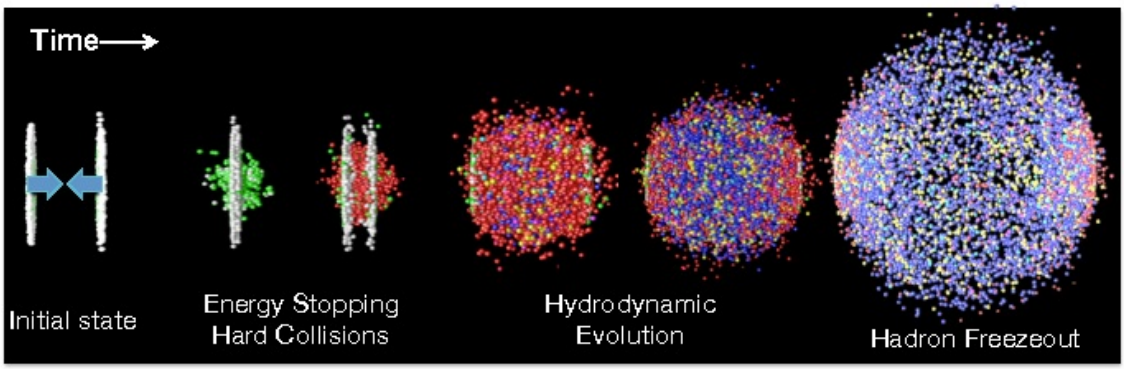

Figure 5: Time evolution of a high energy heavy-ion collision[2]

probe to propagate purely informations of collision process because the photon doesn't participate strong interaction.

Prompt photon

The prompt photon is generated in early state of collisions. The generataion origin is hard scattering, the gluon Compton scattering($q+g \rightarrow q+\gamma$), annihilation by partons($q+\overline{q} \rightarrow g+\gamma$) and so on. These generation ratios are calculated by pQCD.

Thermal photon

The thermal photon is generated in thermal radiation of QGP. This radiation ratio is shown in following:

$$E\frac{dR}{d^3p} = \frac{5}{9}\frac{\alpha\alpha_s}{a\pi^2}T^2 e^{-\frac{E}{T}}\ln(\frac{2.912}{\mathrm{g}^2}\frac{\mathrm{E}}{\mathrm{T}}). \quad (1)$$

This equipment indicates that the thermal photon exists with $e^{-\frac{E}{T}}$ in low p_{T} region. This distribution is important for measuring temperature of QGP. However thermal photon measurement is so difficult on enormous background.

Decay photon

The decay photon is generated by decay of hadron resonance state. This photon constitutes 90% of total photons and its main origin is π^0, η and ω. Therefore it is of importance to understand generation mechanism of decay photon. We noticed the lightest hadron π^0. The property of π^0 is shown in Table 2.

1.5 Previous results at RHIC

Experimental results which indicate production of QGP was confirmed at PHENIX. The PHENIX is one of the experiments with RHIC accelerator at the BNL and performs experiments in heavy-ion

π^0	
Mass	0.135 GeV/c^2
quark	$(u\bar{u}\text{-}d\bar{d})/\sqrt{2}$
J^{PC}	0^{-+}
Decay mode	2γ (98.8%)

Table 2: Property for π^0 meson

collisions[3]. Medium effects such a QGP in nucleus-nucleus collisions are often presented using the nuclear modification factor $R_{\rm AA}$ given as the ratio of the measured nucleus-nucleus invariant yields to the binary collision scaled invariant yields in pp collisions[4]:

$$R_{\rm AA} = \frac{(1/N_{\rm AA}^{\rm evt})d^2N_{\rm AA}/dp_{\rm T}dy}{\langle N_{\rm coll}\rangle/\sigma_{\rm pp}^{\rm inel} \times d^2\sigma_{\rm pp}/dp_{\rm T}dy}, \tag{2}$$

where the $\langle N_{\rm coll}\rangle/\sigma_{\rm pp}^{\rm inel}$ is the average nucleuar thickness function. $R_{\rm AA}$ measures the deviation of nucleus-nucleus data from an incoherent suppression of binary collisions. When $R_{\rm AA}$ is less than 1, it indicates interaction between nucleon and production of QCD matter such as QGP.

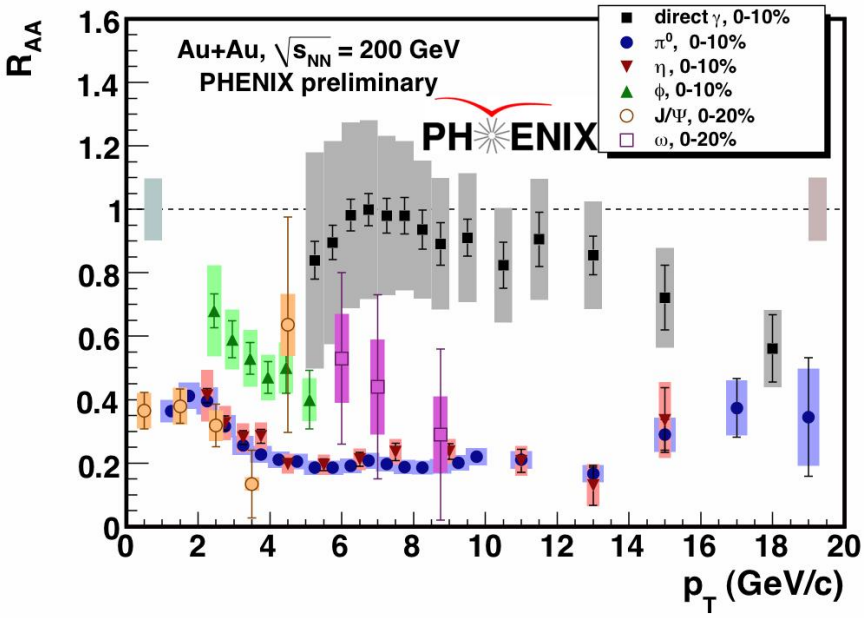

Figure 6: Nuclear modification factor $R_{\rm AA}$ of different mesons and direct photons[5]

Figure 6 shows yields of mesons commencing with π^0 and η are suppressed for $0 < p_{\rm T} < 20$ GeV/c. On the other hand, R_{AA} for direct photon consists with 1 within error for $p_{\rm T} < 13$ GeV/c and

it indicates the yield of direct photon does not change. However it has decreasing trend for $p_{\mathrm{T}} > 15$ GeV/c and is pointed out that photon in initial state is suppressed.

Thermal photon measurement in $\sqrt{s_{\mathrm{NN}}} = 200$ GeV Au-Au collisions has excess in low p_{T} region, approximately $p_{\mathrm{T}} < 3$ GeV/c compared to scaled pp collisions with the number of collisions (Figure 7). We think this excess derives from thermal radiation of hot and dense matter such as QGP. The temperature for QGP is about 220 MeV in the result of fitting by the Boltzmann distribution. This temperature exceeds phase transition temperature of QGP.

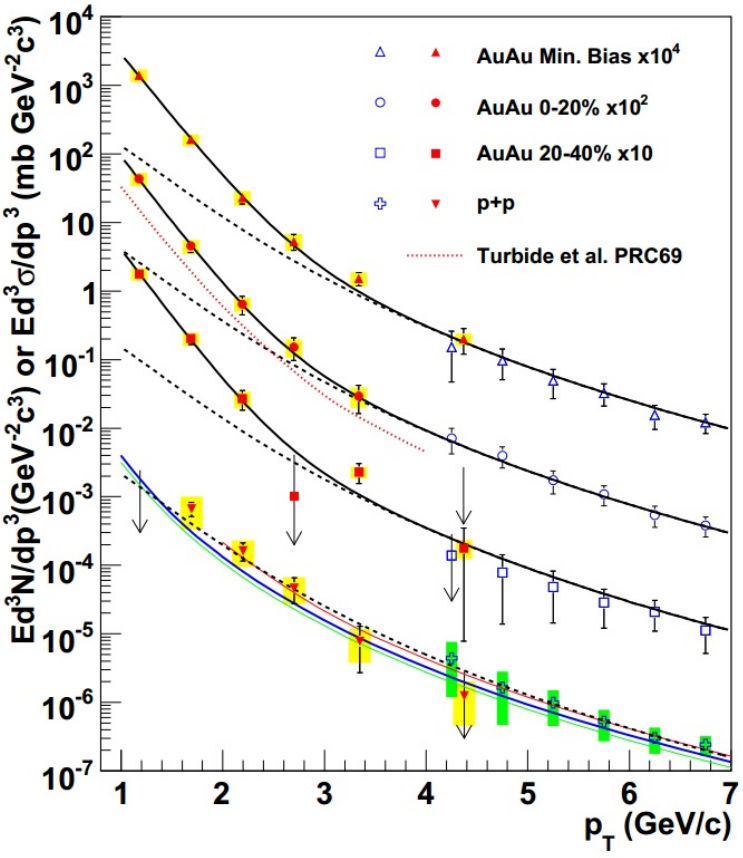

Figure 7: Direct photon spectra[6]

1.6 Motivation

Investigation of QGP which exists in a very early universe, allows to find out the origin of matters. A huge amount of particles are generated in high energy heavy-ion collisions experiment. In such a condition, photon is direct probe and photon measurement is one of the important in order to investigate the property of QGP. Because photon is free of the influence of strong interaction, it can deliver pure information. The study for hadron production in p-Pb collisions data at LHC energy

is able to estimate the influence for QGP production due to a difference in initial condition. In this thesis, it focuses on π^0 meson measurement via two photon decay channel.

We analyzed minimum bias triggered data in $\sqrt{s_{\mathrm{NN}}} = 5.02$ TeV p-Pb collisions with electromagnetic calorimeter PHOS. In order to study it, we estimated accuracy of energy measurement in PHOS with the ratio of energy-to-momentum and measured the π^0 invariant yield.

2 Experimental setup

2.1 LHC accelerator

Large Hadron Collider(LHC) is a two-ring-superconducting-hadron accelerator and collider, which exists under the ground of border between France and Switzerland. It is the Largest accelerator in the world installed in the 26.7 km long circular. It is designed to collide protons with a centre-of-mass energy of 14 TeV ($\sqrt{s} = 14$TeV) and an unprecedented luminosity of 10^{34} cm^{-2}s^{-1}. It can also collide heavy ions with an energy 2.8 TeV per nucleon ($\sqrt{s_{\mathrm{NN}}} = 2.8$TeV) and a peak luminosity of 10^{27} cm^{-2}s^{-1}[7]. The LHC had run from 2009 and ALICE took physical data of proton-proton collisions with a centre-of-mass energy 900 GeV. It took data of proton-proton collisions with a centre-of-mass energy 2.76 TeV and 7 TeV and lead-lead collisions with a centre-of-mass energy 2.76 TeV per nucleon from 2010 to 2012. In addition, data of proton-lead collisions with centre-of-mass energy 5.02 TeV per nucleon was taken in 2013.

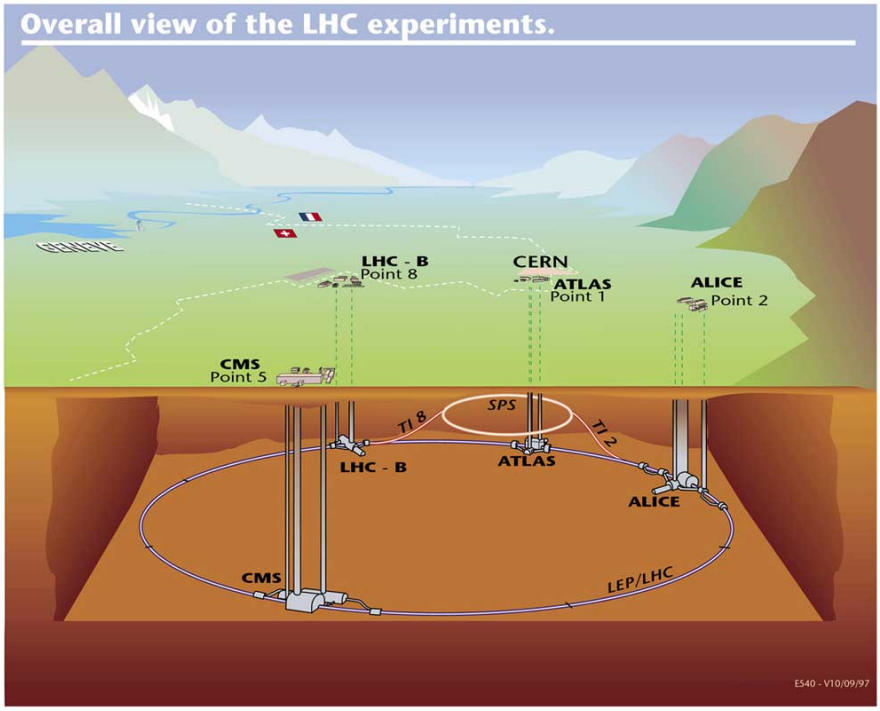

Figure 8: LHC and four main experiments[8]

2.2 The ALICE experiment

A Large Ion Collider Experiment(ALICE) is an experiment at the LHC. The ALICE experiment is designed to address the physics of strongly interacting matter and QGP at extreme values of energy density and temperature in nucleus-nucleus collisions.

ALICE detector is built by a collaboration including currently 1200 physicists and engineers from 132 Institutes in 36 countries[9]. Its overall dimensions are $16 \times 16 \times 26$ m^3 with a total weight of approximately 10000 t. ALICE consists of a central barrel part, which measures hadrons, electrons, photons and a forward muon spectrometer in order to measure the muon. The central part covers polar angles from 45° to 135° and is embedded in a Large solenoid magnet reused from the L3 experiment at LEP[10]. From the collision point, the barrel contains as Inner Tracking System(ITS) of six planes of high resolution silicon pixel detectors(SPD), silicon drift detectors(SDD), and silicon strip detectors(SSD), a cylindrical Time Projection Chamber(TPC), three particle identification arrays of Time Of Flight(TOF), Ring Imaging Cherenkov(HMPID)and Transition Radiation Detectors(TRD) and two electro-magnetic calorimeters, PHOS and EMCal.

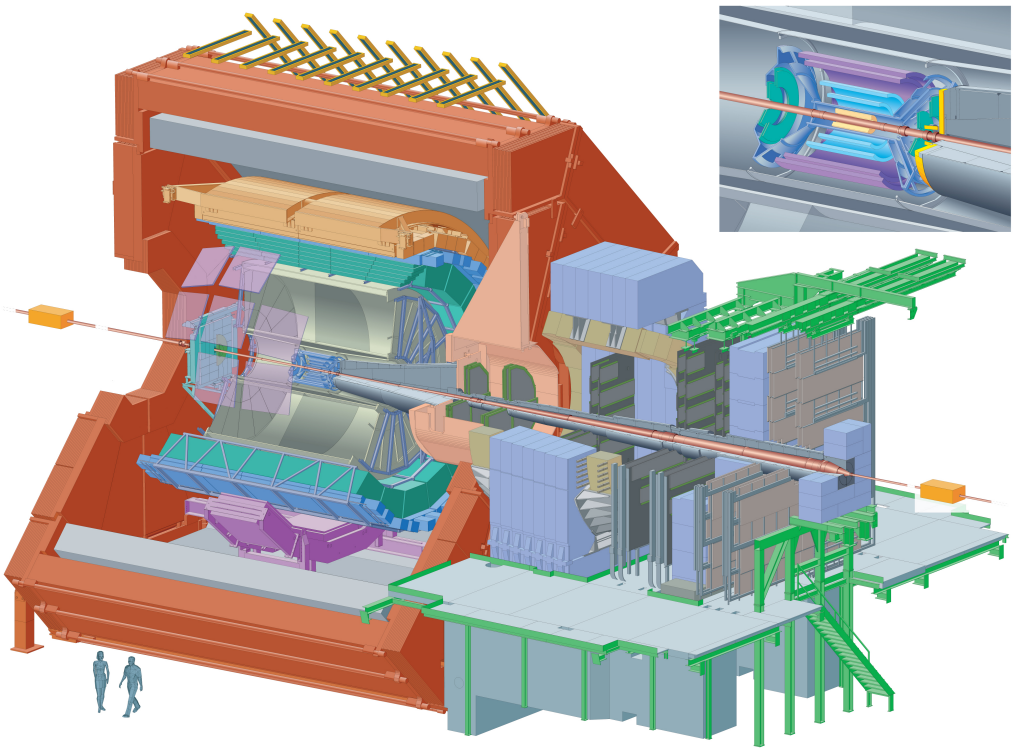

Figure 9: ALICE detector

2.2.1 Charged particle detectors

Inner Tracking Detector(ITS)

The ITS surrounds the beam pipe and covers $|\eta| < 0.9$ in pseudo-rapidity and the full azimuth. The main tasks of the ITS are to localize the primary vertex, to reconstruct the secondary vertices and to track and identify particles. The ITS consists of six cylindrical layers of silicon detectors, located at radii between 3.9 cm and 43 cm. Because of the high particle density expected in heavy-ion collisions

at LHC and in order to achieve the required impact parameter resolution, SPD have been chosen for the innermost two layers, and SDD for the following two layers. The teo outer layers, where the track density is expected to be below one particle per cm^2, are equipped with SSD.

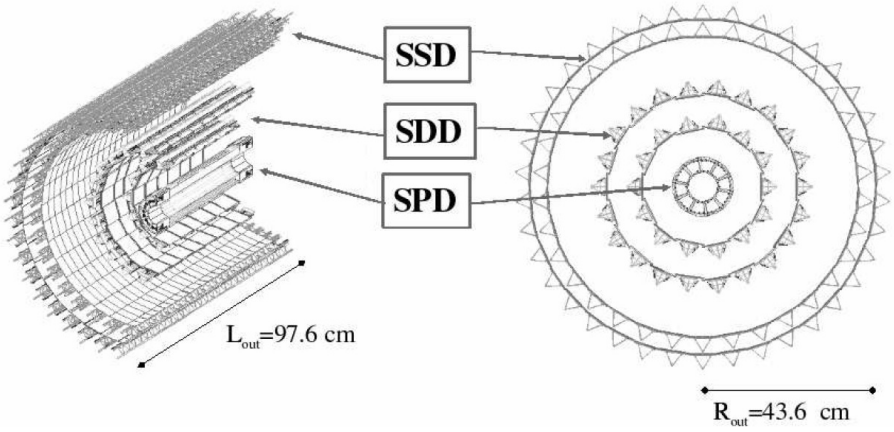

Figure 10: Inner Tracking System[11]

Time Projection Chamber(TPC)

The TPC surrounds the ITS and covers $|\eta| < 0.9$ in pseudo-rapidity and the full azimuth. the TPC is cylindrical in shape, the active volume has an inner radius of about 85 cm, an outer radius of about 247 cm, and an overall length along the beam direction of 500 cm. It is the main tracking detector of the central barrel and is optimized to provide, together the other central barrel detectors, charged particle momentum measurements with good two track separation, particle identification, and the primary and secondary vertices determination. It is filled with the mixture of $Ne/CO_2/N_2$ (85.7%/9.5%/4.8%) in drift volume (90 m^3). It is used to reconstruct the charged particle trajectory in the magnetic field as well as to calculate the particle's specific energy loss dE/dx in the TPC gas. A Large p_T range is covered from low p_T of about 0.1 GeV/c up to 100 GeV/c with good momentum resolution.

2.2.2 Photon detectors

PHOton Spectrometer(PHOS)

The PHOS is one of electro-magnetic calorimeter. Three PHOS modules are installed and covers $|\eta| < 0.12$ in pseudrapidity and the acceptance of $260° < \phi < 320°$ in azimuthal angle. The PHOS consists of PWO crystal and APD readout. The main physics objectives are the test of thermal and dynamical properties of the initial phase of the collision from low p_T direct photon measurements and the study of jet quenching through the measurement of high π^0 in p_T. The detail is described in next section.

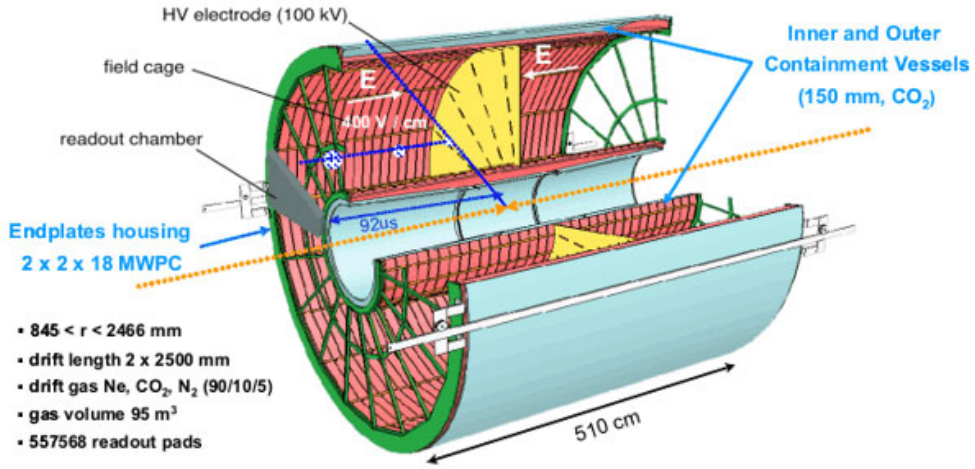

Figure 11: Time Projection Chamber

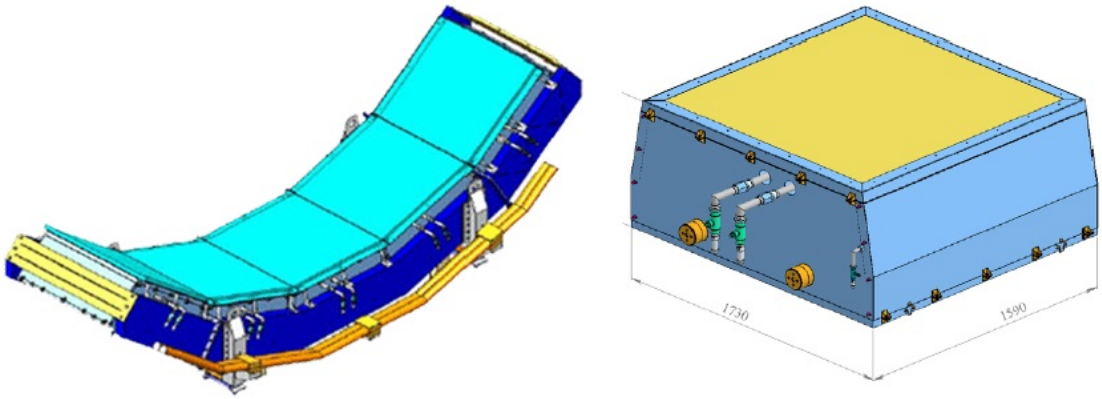

Figure 12: PHOS overview(left) and one PHOS module(right)

Electro-Magnetic Calorimeter(EMCal)

The EMCal is a Large Pb-scintillator sampling calorimeter with cylindrical geometry and covers $|\eta| < 0.7$ with an azimuthal acceptance of $\Delta\phi = 107°$. It is positioned approximately opposite in azimuth to the high-precision PHOS calorimeter. The EMCal has a Large acceptance in order to measure jets quenching which is energy loss of high energy parton.

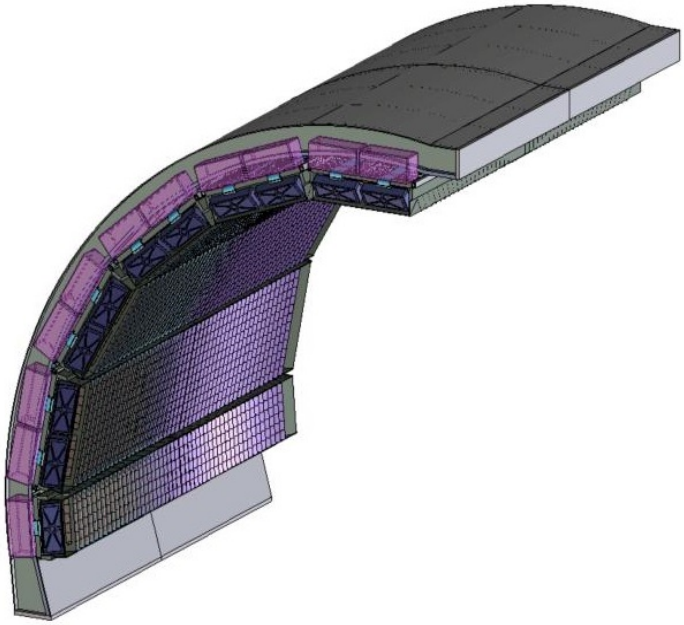

Figure 13: Electro-Magnetic Calorimeter

2.2.3 Forward detector

Zero Degree Calorimeters (ZDC)

ZDC is one of the hadron calorimeter and contains two devices for measuring neutron and proton. Each ZDCs are placed at a distance about 116 m from the collision point. The neutron ZDCs and proton ZDC can measure neutron and proton respectively by separating magnet. The main task is estimation of the number of participants and centrality.

Forward Multiplicity Detector (FMD)

FMD consists of silicon strip detectors and cover the forward regions (-3.4< η <-1.7 and 1.7< η <5.0). It measures the charged particle multiplicity in the forward region.

T0 Detector

T0 detector consists of two Photo Multiplier Tubes(PMT) with the Cherenkov counter. It is

designed to determine the collision time with 50 ps resolution and to detemine the collision vertex with 1.5 cm resolution.

V0 Detector

V0 detector consists of two units of scintillator counters (V0A and V0C). The V0A and V0C are located in 2.8< η <5.1 and -3.7< η <-1.7 respectively. Their information is used as Minimum Bias(MB) trigger.

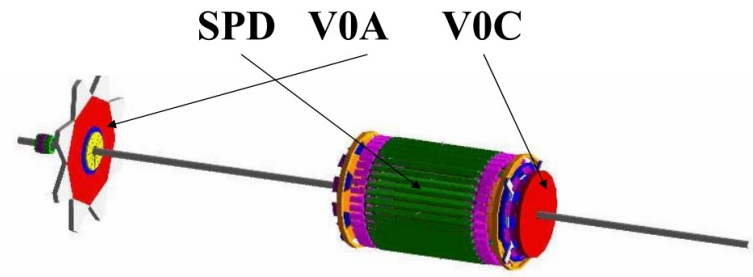

Figure 14: V0 detector and SPD

2.3 Offline analysis framework

The ALICE offline fremawork (AliROOT) has been under development since 1998. It has provided inputs for the Technical Design Reports of all ALICE detectors and for the performance and physics studied presentedi n the ALICE Physics Performance Report[12]. The AliROOT framework is based on Object-Oriented technology and depends on the ROOT framework. Although AliROOT already allows quite detailed and realistic studies of the detectors, it is still under intense development[13].

2.3.1 AliROOT

The AliROOT is the offline framework for simulation, alignment, calibration, reconstruction, visualization, quality assurance, and analysis of experimental and simulated data. The flow of simulation and data reconstruction are shown in Figure 15. It is based on "ROOT" framework. Most of the code written in C++ with some parts in Fortran that are wrapped inside C++ code[14, 15].

2.3.2 GRID

The GRID paradigm implies the unification of resources of distributed computing centers, in particular computing power and storage, to provide them to users all over the world. It allows computing centers to over their resources to a wider community. This allows resources in large collaborations to be shared. The huge amount of date produce by ALICE detector ($\sim$2 PB per year) makes almost unavoidable the necessity of automatized procedures for the (software) reconstruction of the events and for the first steps of the analysis, with the consequent employ of a large mass of computing resources. The worldwide distributed GRID facilities were designed to provide both the computing power and

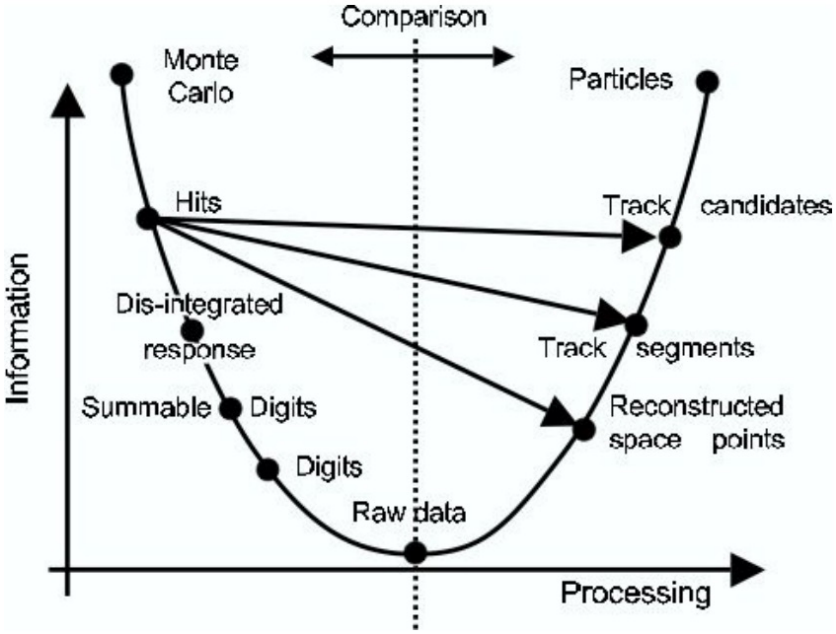

Figure 15: Data Processing framework

the disk space needed to face the LHC software challenge. Hence the need of a GRID oriented analysis code. One of the main advantages in using the GRID is the possibility to analyze a large set of data by splitting a job analysis into many "clone" subjobs running in parallel on different computing nodes. The ALICE VO (Virtual Organization) is made of more than 80 sites distributed worldwide.

3 PHOton Spectrometer

3.1 Basic design

The PHOS is electro-magnetic calorimeter designed to measure the energy and hit coordinates of photons and electrons. At present, The PHOS is installed three modules at a distance of 4.60 m from the interaction point and covers the acceptance of $260^\circ < \phi < 320^\circ$ in azimuthal angle and $|\eta| < 0.12$ in pseudorapidity. Each module has 3584 detection channels in a matrix of 64×56 cells. Each detection channel consists of a $2.2 \times 2.2 \times 18$ cm^3 lead tungsten, $PbWO_4$(PWO), crystal coupled to an Avalanche Photo Diode(APD) and a low-noise Charge-Sensitive Preamplifier(CSP)[16, 17]. The PWO crystal size has been chosen to be almost equal to the Molière radius of the calorimeter medium. The cross-section dimensions of the crystal (2.2 cm) are close of the Molière radius (2 cm). The height of the crystal (18 cm) corresponds to 20 radiation lengths. PHOS operates at a temperature of -25°C at which the yield of PWO crystal is increased by about a factor 3 composed to room temperature. In addition, noise is suppressed in lower temperature. APD has active area of 5×5 mm^2. The spectral response exhibits a maximum at around 600 nm, with a quantum efficiency around 85%. The gain of APD is increasing with decreasing temperature, typically by a factor of 3 at -20°C composed to the gain at 20°C with a bias voltage of 350 V. The CSP on a printed circuit board of area 19×19 mm^2 is mounted to the back side of the APD. It is supplied from +12 to -6 V with power consumption of 64 mW.

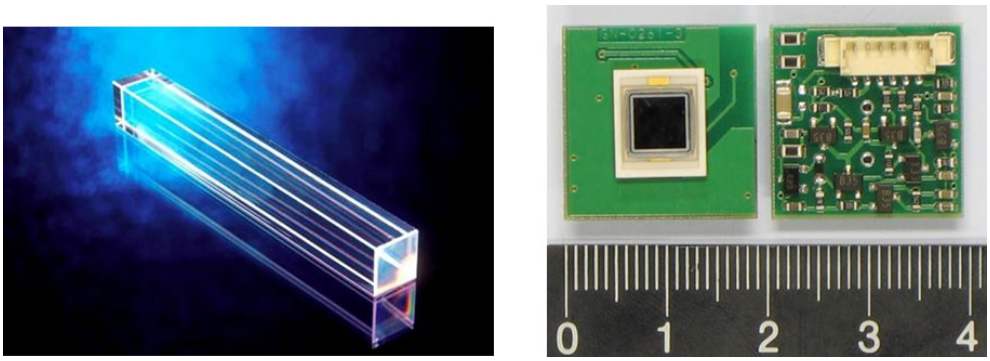

Figure 16: PWO crystal(left) and APD mounted on the preamplifier(right)

3.2 Measurement principle

The energy and position of incoming particles are reconstructed from the amplitudes of signals in the cells measured by the front-end electronics(FEE). Photon and electron measurement in PHOS uses interaction between photon and crystal, which interaction is pair production. This interaction can react by grace of Coulomb field in the nucleus. It is forbidden to react on conservation law of energy and momentum in the vacuum. The pair production can react when photon energy exceeds sum of the mass of electron and positron $2m_ec^2$. The incident high energy photon in PHOS generates electron and positron by pair production and they generate secondary photons by bremsstrahlung. The secondary

photons generate electron-positron pair and this process continues so far as their energies become small less than ionization energy. This phenomenon is called electro-magnetic shower. The number of generated photons is proportional to energy of the incident photon. We can measure the energy to observe scintillation photons induced by generated a mount of electrons and positrons.

Each material has a proper radiation length X_0 which means length so far the energy of incident charged particle becomes 1/e. In the case of photon, it disappear by a interaction and convert to electron-positron pair, but energy of photon does not decrease gradually. Therefore photon intensity corresponds to radiation length of charged particle. We call it conversion length X_p and it has relation as below.

$$X_p = \frac{9}{7} X_0 \tag{3}$$

We can express as a function of material-independent in absorptance of energy and shower extensity. This will enable to compare easily influence on material with radiation length.

Energy resolution

The energy resolution of an electromagnetic calorimeter can be parameterized as

$$\frac{\sigma_E}{E} = \sqrt{\left(\frac{a}{E}\right)^2 + \left(\frac{b}{\sqrt{E}}\right)^2 + c^2} \tag{4}$$

where the energy E is in GeV, a represents the noise, b represents the stochastic term, and c represents the constant term. These parameters were determined as follows by electron beam tests with PHOS prototype for a 3 × 3 detector array, a=0.023 GeV, b=0.031 $\sqrt{\text{GeV}}$, and c=1.11 %[18].

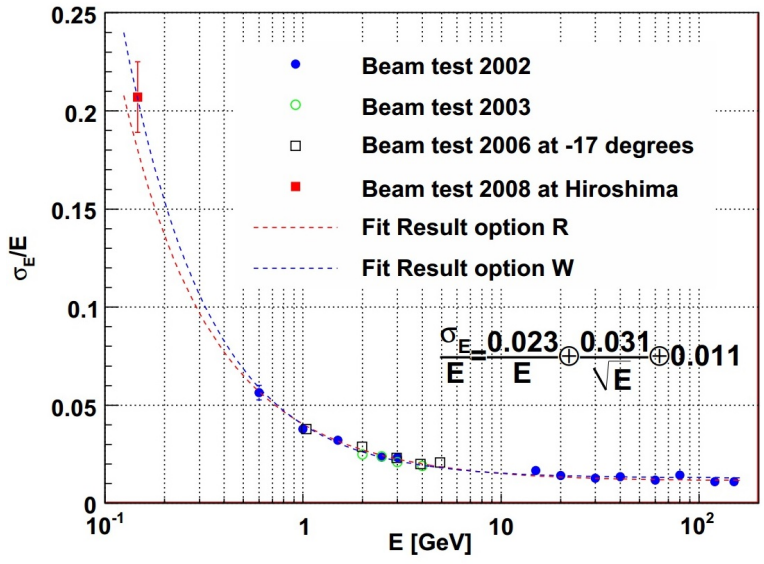

Figure 17: Energy dependence of energy resolution[18]

Position resolution

The position resolution can be parameterized by the following formula:

$$\sigma_{x,y} = \frac{A}{\sqrt{E}} + B, \tag{5}$$

where the energy E is in GeV. In the beam test, the result is shown in Figure 18 and these parameters are found to be $A = 3.26$ mm and $B = 0.44$ mm[19].

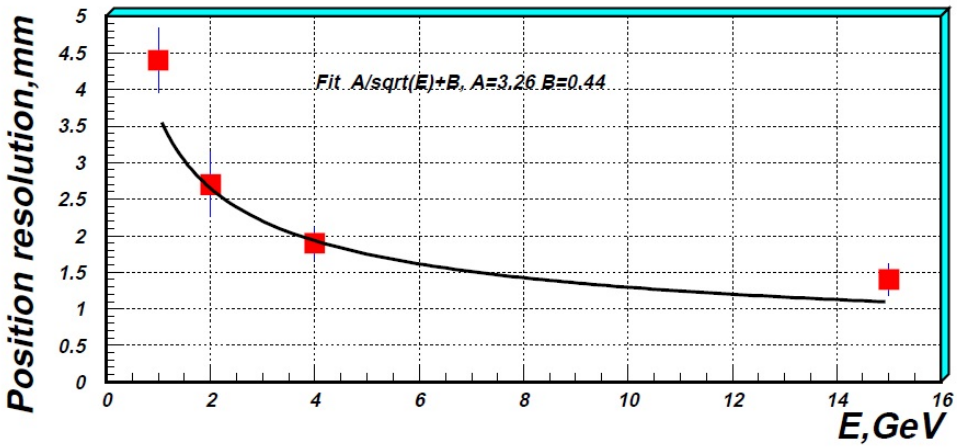

Figure 18: Energy dependence of position resolution[19]

4 Data Quality Assessment(QA)

A data quality assessment is an essential part for the experimental data analysis. It is imperative to check the experimental data quality so as to achieve the reliable result. A response of the calorimeter to particles produced in each collision event, can be produces as a distribution of energy on a rectangular grid which covers a part of solid angle around the collision point. Ideally, the recorded distribution of energy would accurately match the one carried by photons and electrons in an event. As a matte of fact, several problems affect the detector response, e.g. some cells may not function, others are mis-calibrated. These problems occur as dead and noisy cells. These problematic cells are removed or corrected in reconstruction. Therefore we have to take hold of the condition for all cells in each run which represents a unit of data sample, We surveyed all runs and selected good cells.

4.1 Data sample for QA

Analysis presented in the current thesis is based on the event sample collected in 2013 with p-Pb collisions at $\sqrt{s_{\mathrm{NN}}} = 5.02$ TeV (period LHC13b and LHC13c). All events were taken by the data acquisition with the ALICE minimum bias trigger which requires a coinsidence signal in both V0A and V0C and SPD. The number of the minimum bias class was about 80 million events at $\sqrt{s_{\mathrm{NN}}} =$ 5.02 TeV. The analyzed data set is shown in Appendix.

4.2 Cell quality

Some cells in a calorimeter show an abnormally low response compared to others. Such malfunctioning bad cells influence the detector response incorrectly, effectively reducing the acceptance of the detector and leading to loss of signal. An assessment for cell quality is essential in order to identify bad cells.

The calculation of the following four quantities:

1. Total deposited energy in a low energy cluster (0.3 GeV $\leq E_{\mathrm{cluster}} \leq$ 1.0 GeV)
2. Total deposited energy in a high energy cluster (1.0 GeV $\leq E_{\mathrm{cluster}}$)
3. Number of hits in a low energy cluster (0.3 GeV $\leq E_{\mathrm{cluster}} \leq$ 1.0 GeV)
4. Number of hits in a high energy cluster (1.0 GeV $\leq E_{\mathrm{cluster}}$)

The low energy threshold should be the same as the one in the anticipates physics analysis. In this section it was set at 300 MeV, which is a natural choice in order to focus on electro-magnetic shower and therefore discard the signal from minimum ionizing particles(MIPs), which deposit energy in the range of around 250 MeV.

We identified good cells by using a factor. The factor is defined by the following[20].

$$\text{factor} = \frac{[\text{value for a cell}]}{[\text{average over cells}]} \tag{6}$$

The molecule shows number of hits (or total deposited energy) in a cell in a run and the denominator is average of hits (or total deposited energy) over all cells in a run. We claim that a cell is a bad cell

candidate for the current run if its factor is outside an allowed interval defined by two critical values. More precisely, if factor is smaller than lower critical value, the cell is marked as dead, if the factor is greater that the upper critical value, the cell is consideraed as noisy.

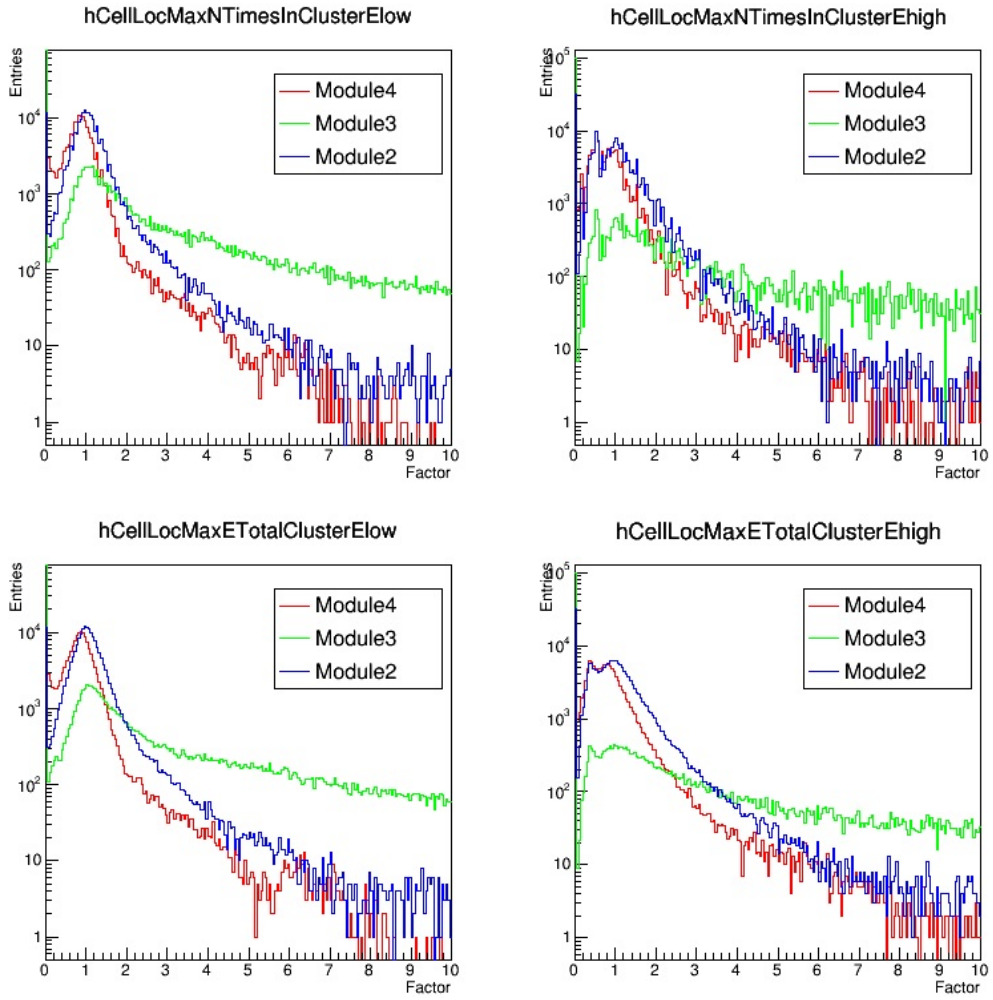

Figure 19: Factor distribution
The low energy range frequency factor(top left), the high energy range frequency factor(top right), the low range energy factor(bottom left), the high energy range energy factor(bottom right).

The factor distributions in each module are presented on Figure 19. Each distribution has irregular and asymmetric shape and there is no evident statistical criteria to discriminate bad and good cells. Too strict criteria would lead to a significant loss of acceptance, while too loose cuts may deteriorate the quality of the data sample. For π^0 spectrum measurement, We choose moderate critical factor values that will lead to excluding only worst cells. The low critical value is 0.05 because it is only necessary to exclude the completely mute cells. On the other hand, it is difficult to determine the

upper critical value for the above reason. To determine the upper cut value quantitatively, we compare the factor distribution in each module and each quantity. The results are shown in Figure 20, 21 and 22.

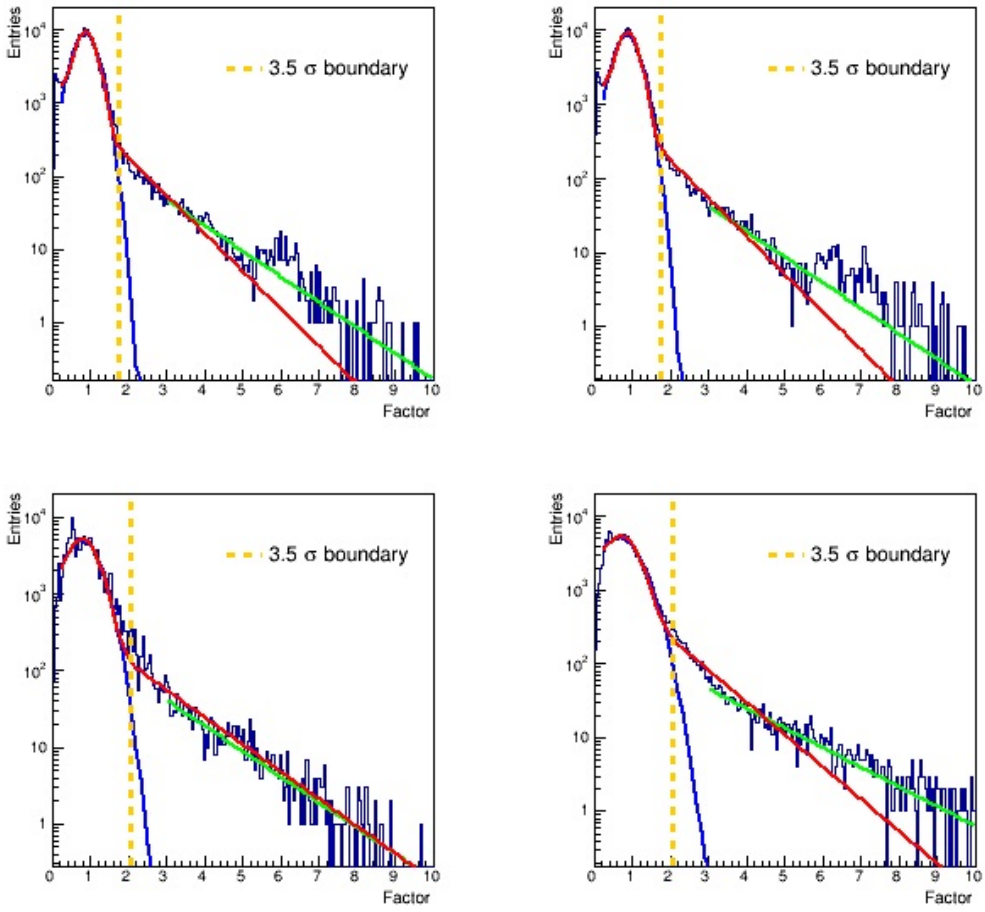

Figure 20: Factor distribution in module4
The low energy range frequency factor(top left), the low energy range energy factor(top right), the high range frequency factor(bottom left), the high energy range energy factor(bottom right). The blue line shows Gaussian fitting, the green line shows exponential fitting, the red line shows a combination of Gaussian fitting and exponential fitting and orange dash line shows 3.5 σ deviation from mean value.

The factor distribution has broad shape (Figure 21) because the module3 has a lot of bad cells, and it is unsuitable for criterion in order to determine good cell. So, we didn't use the module3 for good cell selection.

As a result of combinatorial fitting of Gaussian and exponential, a 3.5 σ deviation from mean value was 2.5 at a maximum. So, we determined the upper critical value as 2.5.

In this way we determined critical factor values: the lower cut value is 0.05 and the upper cut

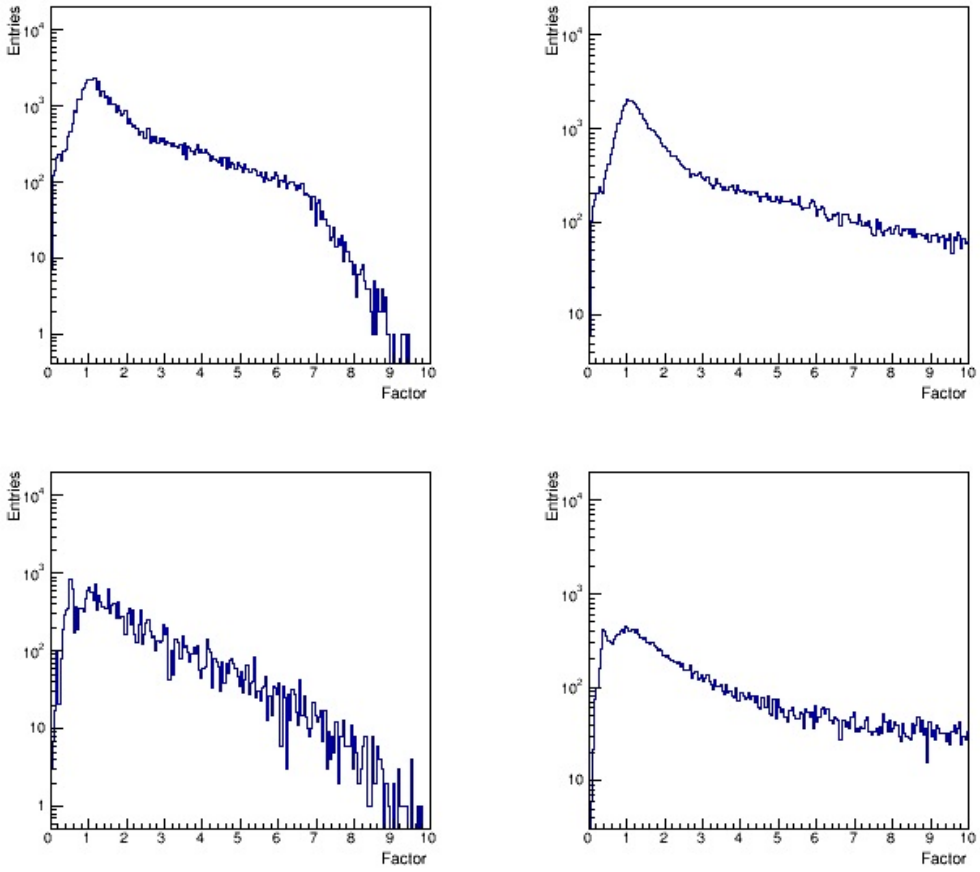

Figure 21: Factor distribution in module3
The low energy range frequency factor(top left), the low energy range energy factor(top right), the high range frequency factor(bottom left), the high energy range energy factor(bottom right).

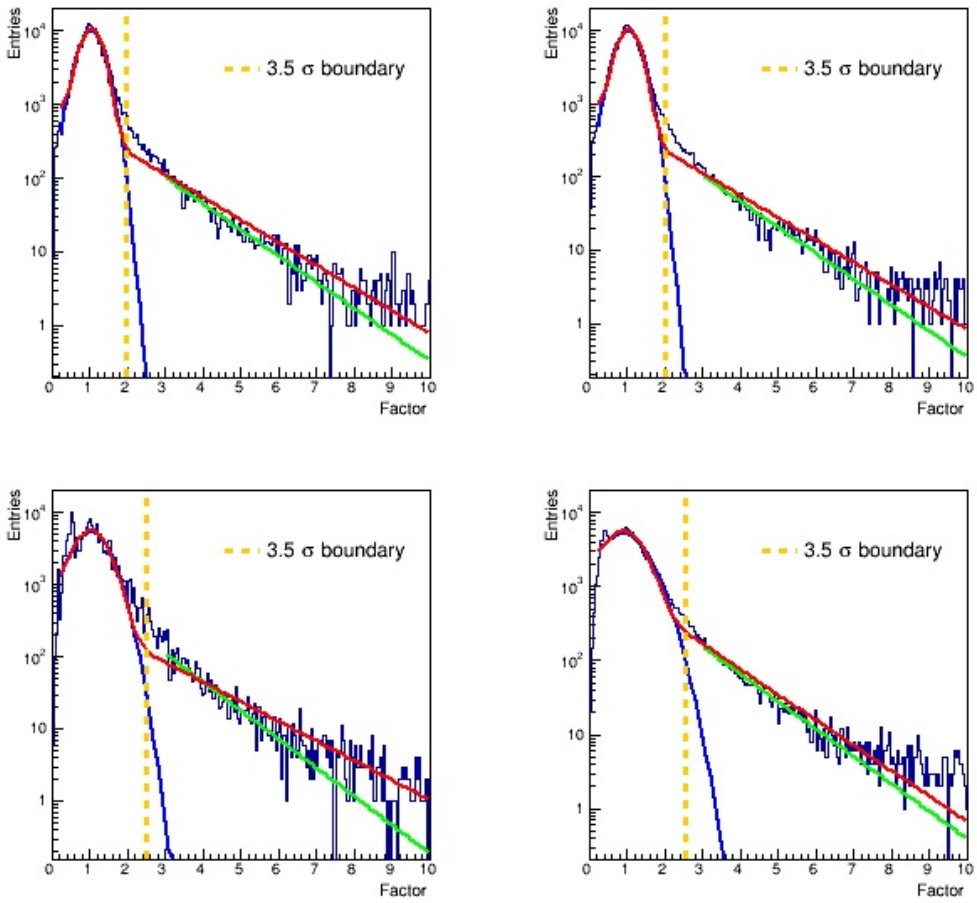

Figure 22: Factor distribution in module2
The low energy range frequency factor(top left), the low energy range energy factor(top right), the high range frequency factor(bottom left), the high energy range energy factor(bottom right). The blue line shows Gaussian fitting, the green line shows exponential fitting, the red line shows a combination of Gaussian fitting and exponential fitting and orange dash line shows 3.5 σ deviation from mean value.

value is 2.5. The factor is calculated in cell-by-cell and run-by-run in surveying all runs excluding low statistics ($< 10^5$ events) runs to reduce statistics fluctuation. The criteria of good cell selection depend on statistics and low statistics results in large fluctuation. For example, a good cell is misidentified as dead cell when it has no hits incidentally all along of low statistics and no output signals. To avoid such a mistake in judgment, it needs to decide a low limit in event count per run. we counted the number of good cells per run and estimated run statistics dependence of the number of good cells(Figure 23).

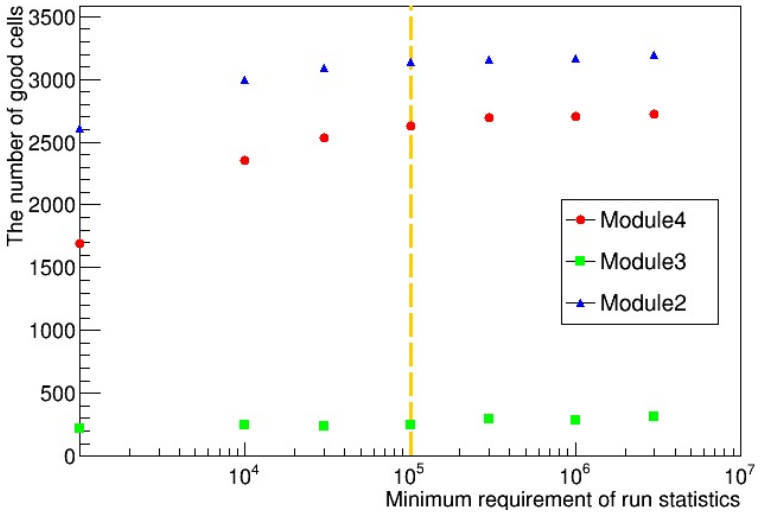

Figure 23: Run statistics dependence of the number of good cells per run

In the result, the statistics fluctuation is small and the number of good cells are almost constant when we use run which has more than about 10^5 events statistics. So, We decided to use runs which has at least 10^5 events for selecting cell quality.

We determined cell quality with using above method and runs which have more than 10^5 events. Figure 24 demonstrates occupancy of all PHOS modules. Here the color is used as indication of degree of problem (red stands dead cell, blue for noisy and white are the normal cell).

We can see the module3 has many dead and noisy cells. So, It is difficult to analyze. As a result, we decided not to use the module3 for analysis. From next section, We will show results with only module4 and module2.

4.3 Run selection

Data taking and detector condition may evolve with time. It is important to estimate the periods when the PHOS and data taking work stability. In particular, the bad channel list may be not persistent because different modules of the detector may fail and be repaired afterwards. A way to monitor this long-term evolution is to study the dependence of basic physics observable versus time. In this thesis, the good runs were selected by following observables.

1. Average cluster energy

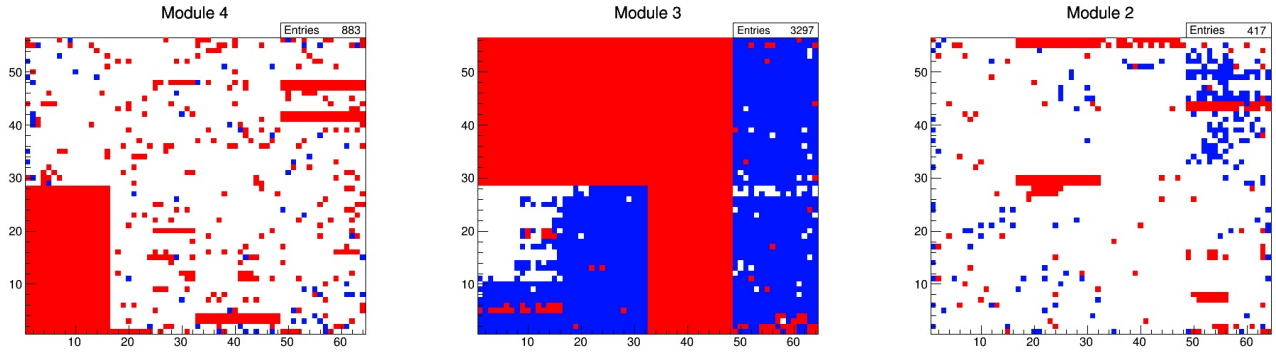

Figure 24: PHOS occupancy map
The horizontal axis are φ direction and vertical axis are beam axis. Color indicates that red are the dead cells, blue are the noisy cells and white are the normal cells.

2. Average number of reconstructed clusters per event

3. Average number of cells per reconstructed cluster

These observables are delivered from the physics objects reconstructed in the PHOS. The selection criteria for the clusters should preferably be the same as used in the physics analysis. The cluster energy was required to be above the minimum ionization energy $E_{\text{cluster}} > 0.3$ GeV and the minimum number of cells in a cluster was 3 cells to reduce the contribution of non-photon clusters and noise.

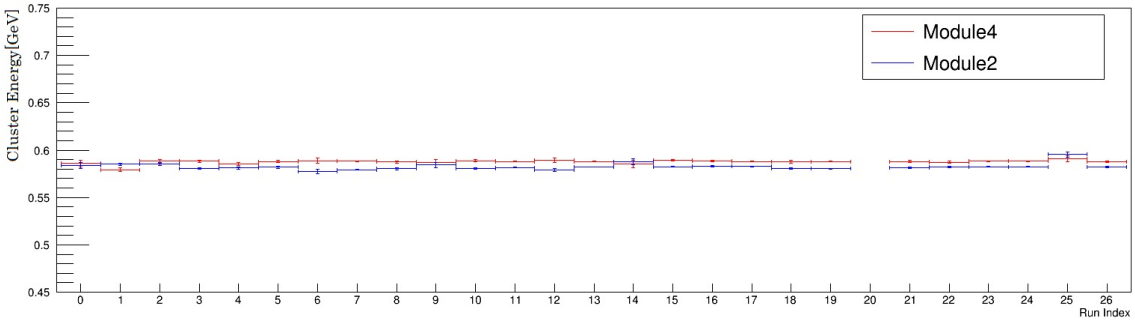

Figure 25: Average cluster energy

These observational results (Figure 25, 26 and 27) show the average cluster energy, the number of clusters per event and the number of cells per event, respectively. Most runs are stable in each module but some runs have abnormally behavior. Run index No.20 is empty because this run does not include PHOS. We can notice that run index No.1, 14 and 25 are abnormally compared to other runs. These runs may cause a negative effect for results. We decided to exclude these 4 runs in this thesis.

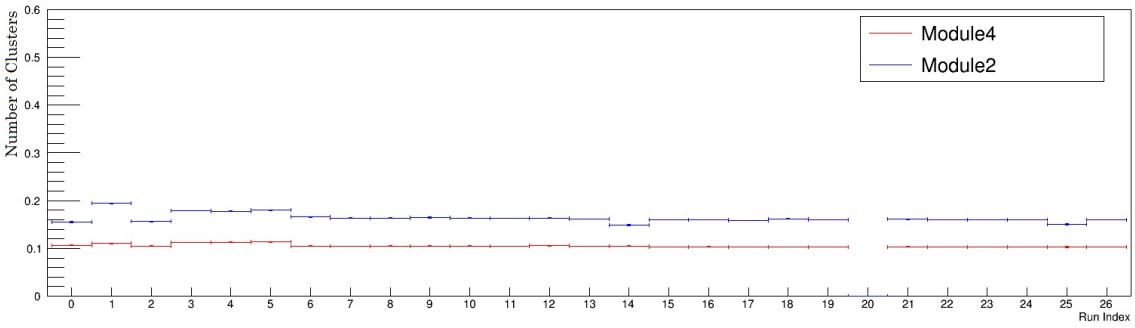

Figure 26: Number of clusters per event

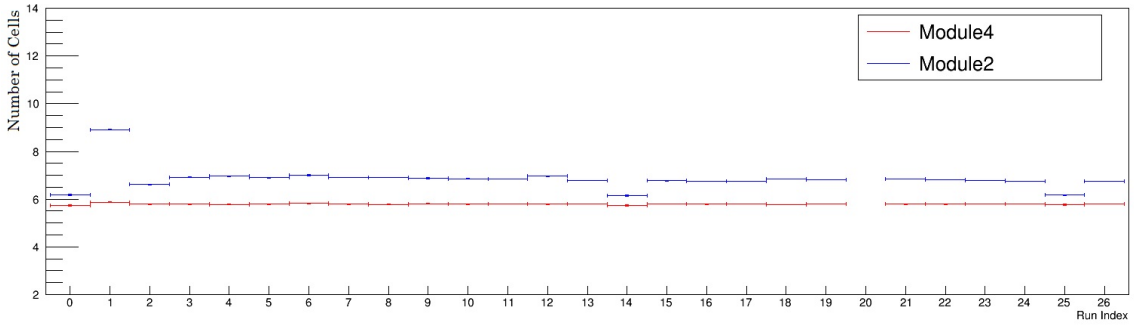

Figure 27: Number of cells per cluster

5 Ratio of energy to momentum for electron

It is estimable for accuracy of PHOS energy calibration with energy-to-momentum ratio (E/p) because the electron initiates same reaction with photon in PHOS. Here, energy is measured by PHOS and momentum is measured by TPC. The E/p is expected to become 1 because electron deposits total energy in PHOS. In reality, however, the E/p does not become 1 due to diverse causes: bremsstrahlung, energy loss in reconstruting and so on.

5.1 Cluster and track selection

For energy measurement in PHOS, we applied the PHOS bad map in addition to the same cut criteria in QA ($E_{\mathrm{cluster}} > 0.3\mathrm{GeV}$ and $N_{\mathrm{cell}} > 2$). We used particle identification by TPC and shower shape cut in order to identify electron candidate. In addition to these cuts, identical electron was required a conformity of PHOS cluster with TPC track.

5.1.1 Electron identification in TPC

The TPC is main device for tracking of charged particles and particle identification by energy loss ($\mathrm{d}E/\mathrm{d}x$). Figure 28 shows the $\mathrm{d}E/\mathrm{d}x$ of charged tracks versus their momentum measured by the TPC in p-Pb collisions. The lines are a parametarization of the detector response based on the Bethe-Bloch formula:

$$-\langle\frac{dE}{dx}\rangle = Kz^2\frac{Z}{A}\frac{1}{\beta^2}[\frac{1}{2}\ln\frac{2\mathrm{m_e}\mathrm{c}^2\beta^2\gamma^2\mathrm{T_{max}}}{\mathrm{i}^2} - \beta^2 - \frac{\delta(\beta\gamma)}{2}]. \tag{7}$$

In order to identify the articles, the measured $\mathrm{d}E/\mathrm{d}x$ is compared with the expected $\mathrm{d}E/\mathrm{d}x$ of the different particle species. In the figure 28 this corresponds to the solid lines. For particle identification the distance to lines is expressed in terms of the detector resolution (σ):

$$n\sigma = \frac{\mathrm{d}E/\mathrm{d}x_{\mathrm{measured}} - \mathrm{d}E/\mathrm{d}x_{\mathrm{expected}}}{\sigma} \tag{8}$$

Where the resolution depends on the track properties, better the number of clusters used for $\mathrm{d}E/\mathrm{d}x$ estimate. To get the TPC $\mathrm{d}E/\mathrm{d}x$ signal, the function "GetTPCsignal()" is provided in the ESD and AOD track classes[23]. In this thesis the cut criterion for electron identification is that the number of sigma for electron ($\sigma_{\mathrm{electron}}$) is $-2 < \sigma_{\mathrm{electron}} < 3$.

5.1.2 Shower shape cut

The interaction between particle and matter is different by particle species. Therefore a response of PHOS depends on particles. The elastic collisions with nucleus and electrons inside of the atom is dominant in the interaction of charged particles such as muon and charged pion. The bremsstrahlung is dominant interaction in the electron and positron and they invoke electro-magnetic shower to trigger it. The interaction between high energy photon and matter is electro-magnetic shower triggered by pair-production. A cut using this difference in PHOS response is shower shape cut. However the electron has most of the same response as photon in the PHOS, because their interactions bring on same electro-magnetic shower after all. This is effective cut for selecting photon cluster and electron

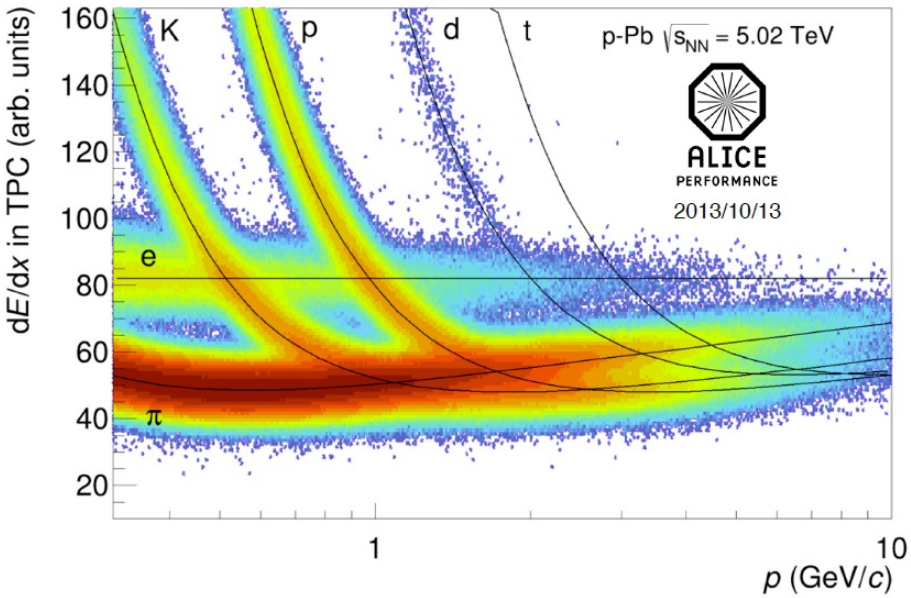

Figure 28: dE/dx distribution in TPC

cluster. We expect to be able to separate photon and electron from other particles with use of a distinctive shower shape for photon and electron cluster.

The shower shape for photon and electron cluster is studied by simulation and real data. In this analysis, We used shower shape of photon and electron cluster to resemble ellipse and estimated cluster shape by introducing following equation and variable.

$$R2 = 0.5 \times \frac{(l1 - l1Mean)^2}{(l1Sigma)^2} + 0.5 \times \frac{(l2 - l2Mean)^2}{(l2Sigma)^2} - 0.5 \times c \cdot \frac{(l1 - l1Mean)(l2 - l2Mean)}{(l1Sigma)(l2Sigma)} \quad (9)$$

where l1 is M20 (short axis of ellipse) and l2 is M02 (long axis of the ellipse). These M20 and M02 are shown in Figure 29. Other parameters are defined as below (E is energy in GeV).

$$l1Mean = 1.123 + 0.123 \times exp(-E \times 0.246) + 5.3 \times 10^{-3} \times E$$
$$l2Mean = 1.531 + 9.508 \times 10^{6}/(1 + 1.087 \times 10^{7} \times E + 1.734 \times 10^{6} \times E^2)$$
$$l1Sigma = 4.447 \times 10^{-4} + 6.998 \times 10^{-1}/(1 + 1.225 \times E + 6.786 \times 10^{-7} \times E^2) + 9 \times 10^{-3} \times E$$
$$l2Sigma = 6.482 \times 10^{-2} + 7.602 \times 10^{10}/(1 + 1.53 \times 10^{11} \times E + 5.012 \times 10^{5} \times E^2) + 9 \times 10^{-3} \times E$$
$$c = -0.35 - 0.550 \times exp(-0.391 \times E)$$

When the R2 of cluster is R2 $< 2.5^2$, the cluster is assumed that it is a photon or electron cluster. In ALICE PHOS group, the cut parameter (R2 $< 2.5^2$) is general[21, 22].

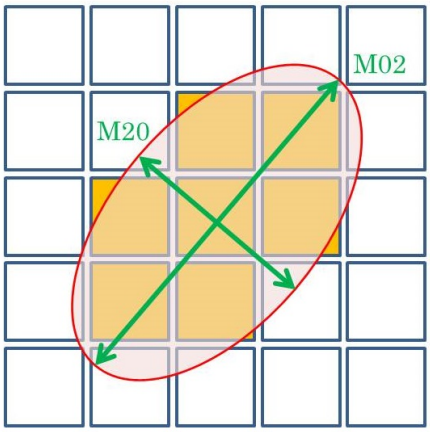

Figure 29: Shower shape of photon

5.2 Mean and sigma for E/p ratio peak

The E/p ratio spectra are shown in Figure 30 and 31. As you can see, all spectra have peak at E/p = 1 up to 5 GeV/c. In low p_{T} regions ($p_{\mathrm{T}} < 0.9$ GeV/c), it has a peak and background contamination around the peak due to stemming from not being able to separate well electrons and other particles. Not only small contribution of electrons but also larger contribution of other particles exist around $E/p = 0.3$ in 0.9 GeV/c $< p_{\mathrm{T}} <$ 1.3 GeV/c. This is caused by miss-identification in TPC. You can find that there is crossed line between electron and proton around $p_{\mathrm{T}} = 1$ GeV/c in Figure 28 and electron and proton at about 1 GeV/c lose almost the same energy in TPC. In addition, other crossed lines exist at $p_{\mathrm{T}} = 2$ GeV/c and 3 GeV/c. Therefore, protons are predominant in the larger peak at $p_{\mathrm{T}} = 1$ GeV/c and hadrons also form it in other p_{T} regions.

The electron E/p peak is fitted by the Gaussian and polynom of the third order and the pesk position and width compared to before and after calibration are shown in Figure 34 as a function of p_{T}. The E/p ratio spectra after calibration are presented on Figure 32 and 33. In the before calibration (see open circle markers in Figure 34), the position has slightly smaller than 1 in entire p_{T} range. It has about 2 % difference from $E/p = 1$. Especially in low p_{T} region, it has huge deviation. This deviation is caused by non-linealiry effects such as bremsstrahlung and energy loss in cluster reconstruction. We corrected it because it harms the precise energy measurement.

In the result of after calibration (spectra are shown in Figure 32 and 33), it is consistent with E/p = 1 within errors in nearly the entire p_{T} regions (see full circle markers in Figure 34). Moreover, the peak width has smaller value in higher p_{T} regions in both before and after calibration (Figure 35), and it indicates the PHOS energy resolution improves in higher p_{T}.

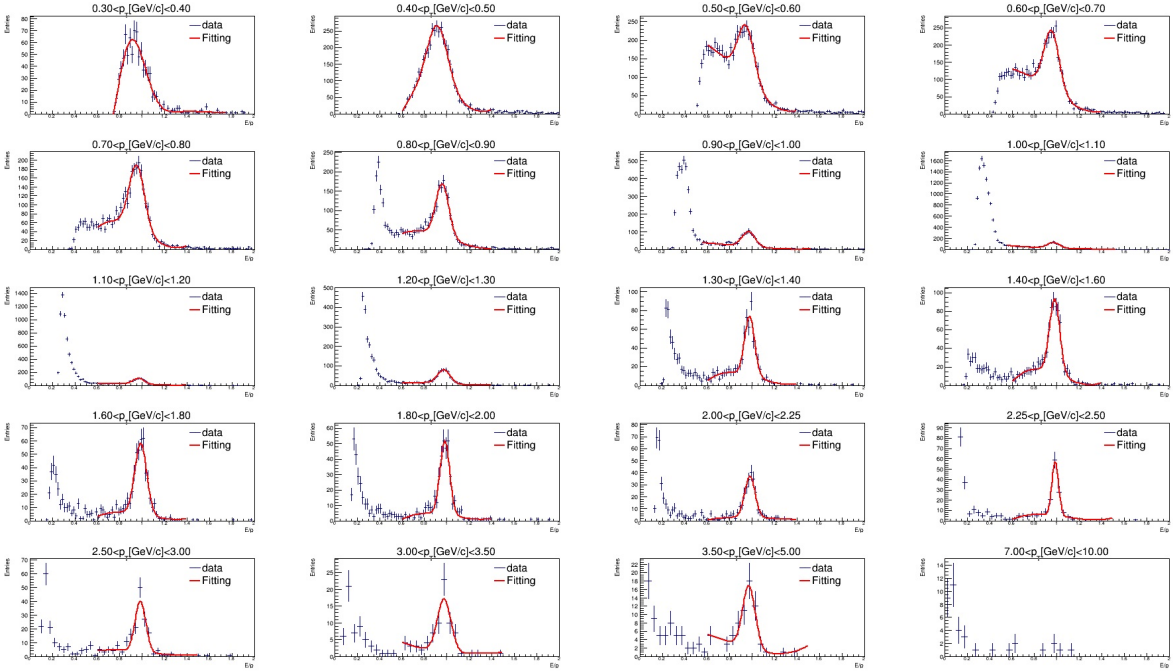

Figure 30: E/p ratio spectra in module4

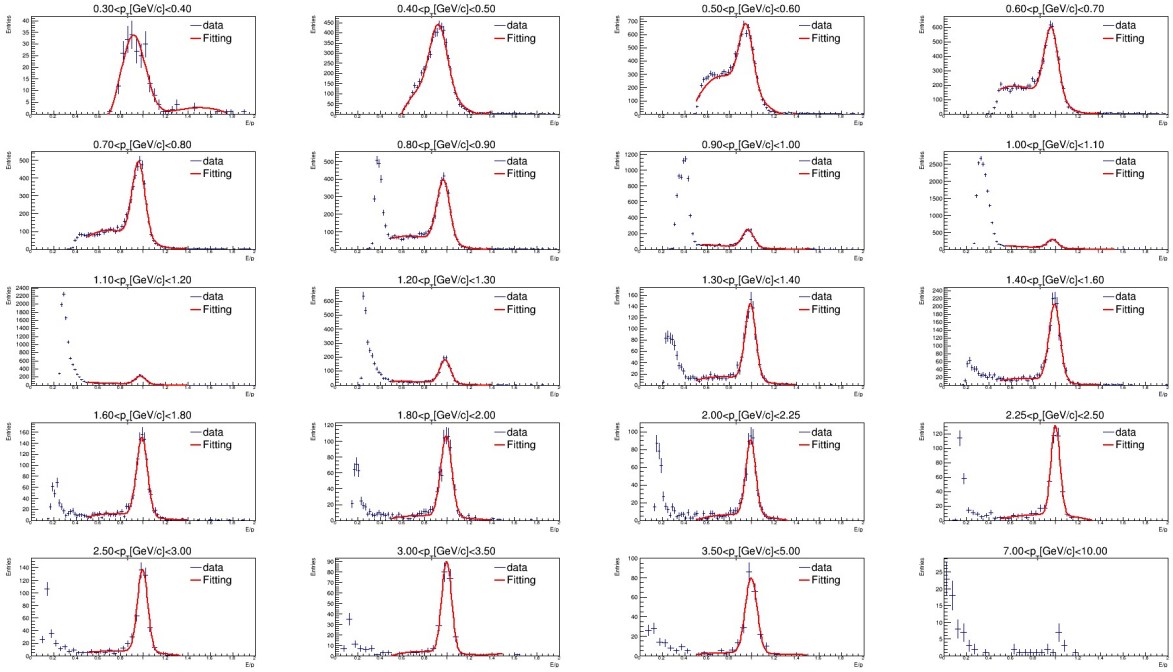

Figure 31: E/p ratio spectra in module2

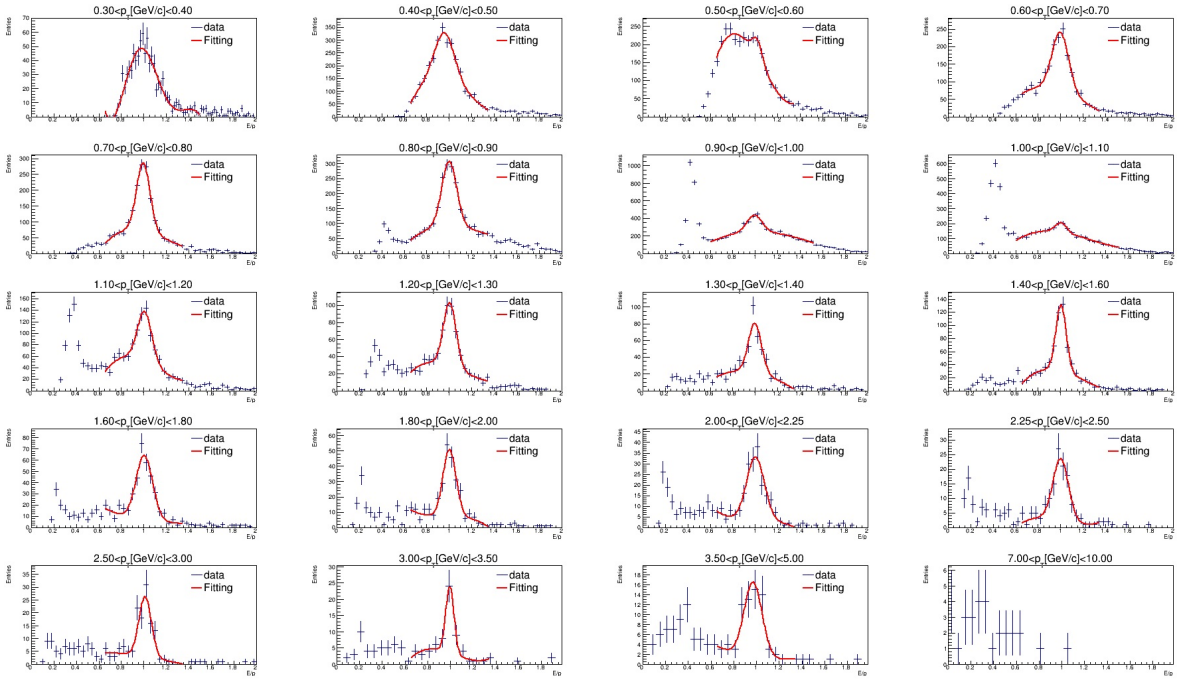

Figure 32: E/p ratio spectra in module4 after calibration

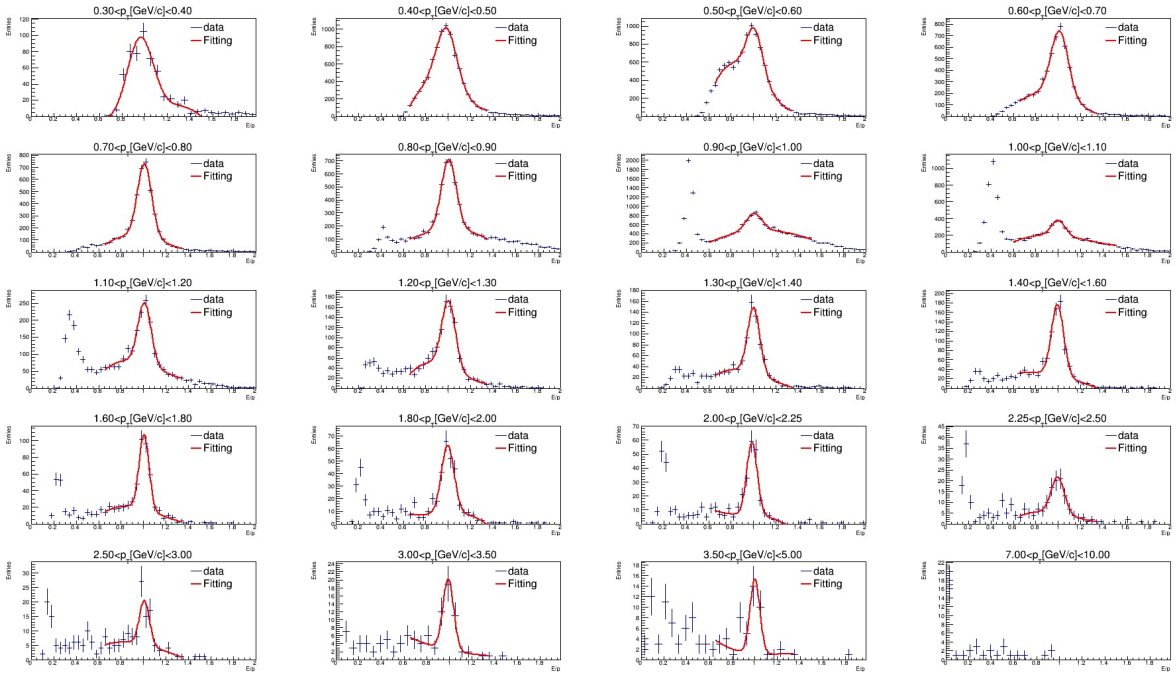

Figure 33: E/p ratio spectra in module2 after calibration

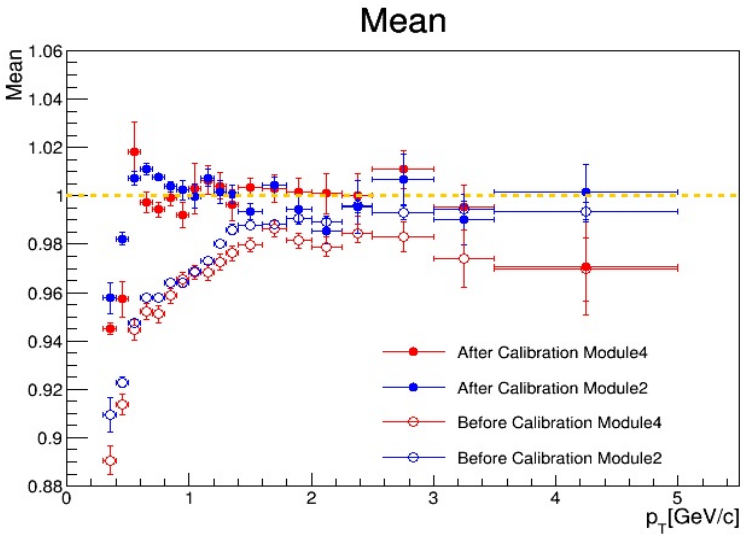

Figure 34: Peak position for E/p ratio
Open circles show before calibration and full circles show after one.

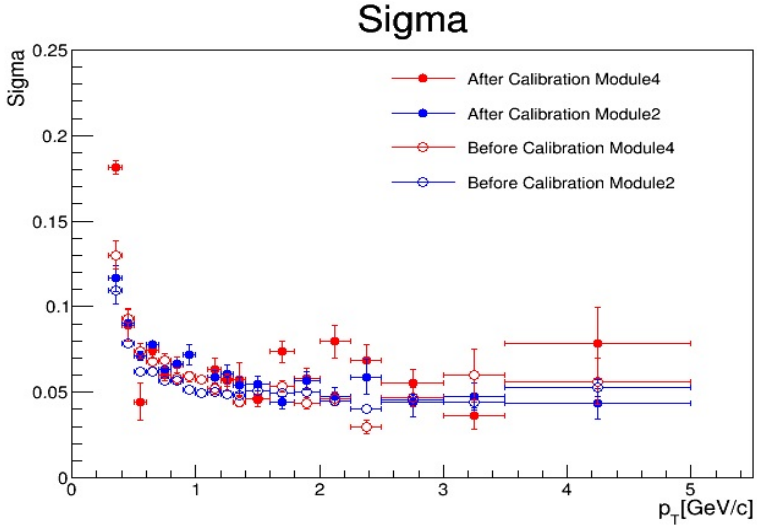

Figure 35: Peak width for E/p ratio
Open circles show before calibration and full circles show after one.

6 Measurement of π^0

6.1 Photon candidate

We selected photon candidate clusters with energy threshold, the number of cells, shower shape cut and CPV cut. The energy threshold, the number of cells and shower shape cut were explained above. This section provides an account for CPV cut.

Charged Particle Veto(CPV) cut is to reject a contamination of charged particle especially electron and positron. As explained above, photon and electron behave the same way in the PHOS. Therefore it is impossible to identify photon and electron in the only PHOS. So, we identify the origin of cluster by using a existence or non-existence of track in TPC. The TPC existing on the inner side of the PHOS reconstructs track for charged particle. We are able to determine whether the cluster is photon origin by using the track information. We applied the cut that ignoring the cluster which distance between track and cluster is within 5 cm.

6.2 Reconstruction of π^0 meson

The neutral meson decays at once soon after generated in collisions. Hence, it is impossible to detect it directly. The analysis method for such particles is reconstructing invariant mass from particles after decay and counting the number of parent particles. We explain it in this section.

The π^0 meson is reconstructed from two photons detected by PHOS in each same event. Invariant mass M_{12} is calculated by the following formula:

$$M_{12} = \sqrt{E_1^2 + E_2^2 - (\overrightarrow{p_1} + \overrightarrow{p_2})^2} = \sqrt{m_1^2 + m_2^2 + 2(E_1 E_2 - \overrightarrow{p_1} \cdot \overrightarrow{p_2})} \tag{10}$$

where E_i, $\overrightarrow{p_i}$ and m_i are energy, four-momentum and rest mass, respectively. In the case of photon, it doesn't have a mass and it becomes $E = p$. Above equation can be simplified as follow:

$$M_{\pi^0} = \sqrt{2E_1 E_2(1 - \cos\theta_{12})} \tag{11}$$

where θ_{12} is opening angle between two photons. The PHOS can measure only the energy and position. But π^0 meson has a short lifetime and decays at once soon after generated in collision point. Therefore we can calculate the opening angle by following to assume the vertex of opening angle as collision point.

$$\cos\theta_{12} = \frac{\overrightarrow{r_1} \cdot \overrightarrow{r_2}}{|\overrightarrow{r_1}||\overrightarrow{r_2}|} \tag{12}$$

where $\overrightarrow{r_i}$ is position measured in PHOS. The reconstructed invariant mass distribution is provided in Figure 36.

6.3 Raw yield extraction

We extracted π^0 raw yield from two-photon invariant mass distribution. The invariant mass spectrum was fitted by the sum of the Gaussian and a polynom of the second order:

$$f(x) = A \cdot exp(\frac{-(m-M)^2}{2\sigma}) + a_0 + a_1 x + a_2 x^2 \tag{13}$$

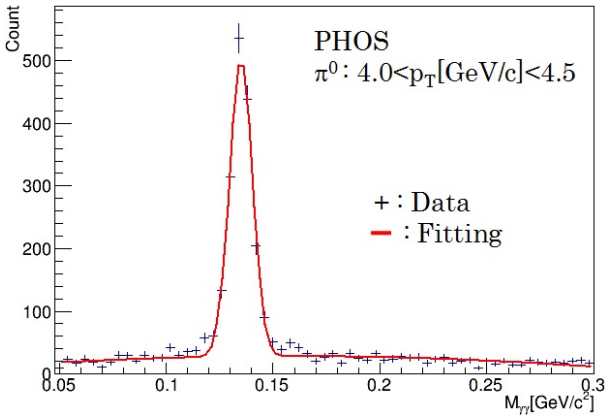

Figure 36: Invariant mass spectrum in selected p_{T} slice

where A, M and σ show the height of peak, the mean value of peak and the peak width, respectively. The fitting result is shown by red line.In this case the number of reconstructed π^0's can be found as an integral under the Gaussian part of the fitting function:

$$N = \frac{A \cdot \sigma \cdot \sqrt{2\pi}}{\delta m} \tag{14}$$

where δm is bin width. In addition, the error is calculated by

$$dN = N \cdot \sqrt{\left(\frac{dA}{A}\right)^2 + \left(\frac{d\sigma}{\sigma}\right)^2}. \tag{15}$$

The reconstructed invariant mass spectra are shown in Figure 37 and 38. As you can see, almost spectra up to $p_{\mathrm{T}} = 14$ GeV/c have fine peak around π^0 mass region and have background corresponding to each p_{T} range. The raw yield spectrum of the reconstructed π^0 was obtained from invariant mass spectra is shown in Figure 39.

6.4 Efficiency calculation

The π^0 raw yield spectrum has to be corrected for the PHOS acceptance, for the probability of the π^0 loss due to photon conversion in the medium, and for the efficiency of the π^0 number extraction from the invariant mass spectra of cluster pairs. The efficiency was calculated in Monte Carlo simulations with ALICE official production and a single π^0 per event. The ALICE official production is anchored LHC13b and c, and single π^0 is generated in flat p_{T} spectrum in range 10 to 25 GeV/c in uniform distributions over the azimuthal angle $0° < \phi < 360°$ and rapidity $|y| < 0.5$.

The acceptance and reconstruction efficiency were calculated by following formula. The PHOS acceptance has been chosen to be slightly larger ($|\eta| < 0.13,\ 250° < \phi < 330°$) than the PHOS aperture ($|\eta| < 0.12,\ 260° < \phi < 320°$) to avoid the boundary effects. The simulation with the real ALICE geometry were performed, the simulated data were reconstructed with the same condition

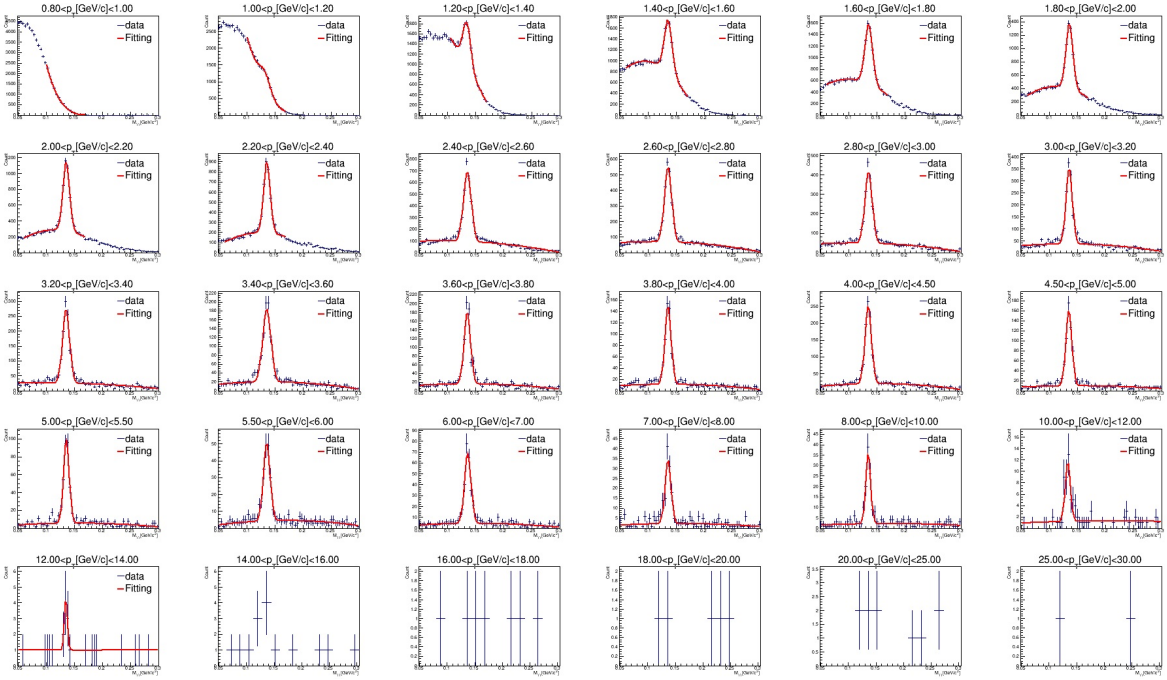

Figure 37: Invariant mass spectra in module4

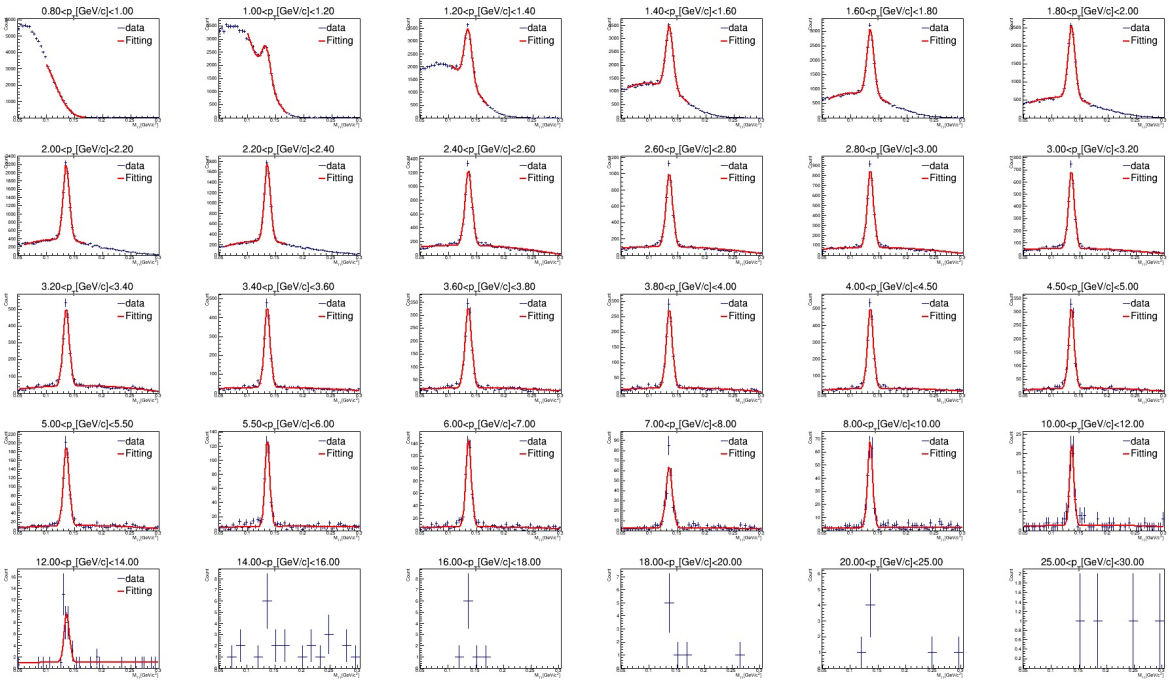

Figure 38: Invariant mass spectra in module2

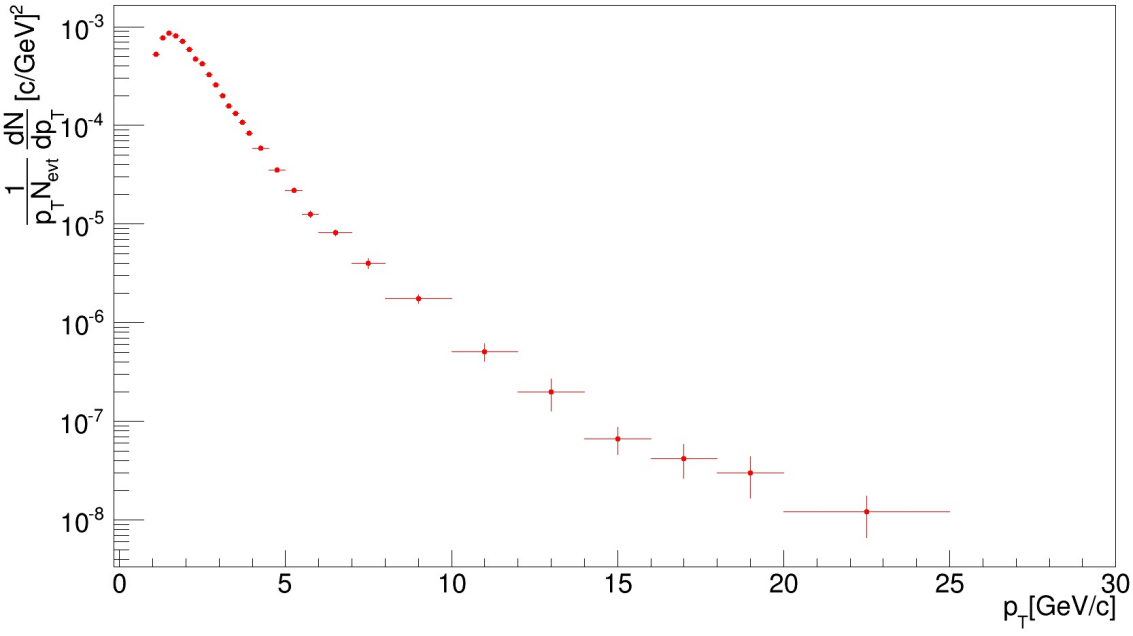

Figure 39: π^0 raw yield

data as those used in this simulation and in the reconstruction of the real PHOS data. The efficiency of the π^0 reconstruction in PHOS in the p_{T} range from 0 to 25 GeV/c is shown in Figure 40.

$$\varepsilon_{\mathrm{Acc}} = \frac{\pi^0 \text{ going to within PHOS acceptance}(|\eta| < 0.13,\ 250^\circ < \phi < 330^\circ)}{\text{Generated } \pi^0(|\eta| < 0.5,\ 0^\circ < \phi < 360^\circ)} \tag{16}$$

$$\varepsilon_{\mathrm{Rec}} = \frac{\pi^0 \text{ reconstructed in PHOS}}{\pi^0 \text{ going to within PHOS acceptance}(|\eta| < 0.13,\ 250^\circ < \phi < 330^\circ)} \tag{17}$$

$$\varepsilon_{\mathrm{Acc\times Rec}} = \varepsilon_{\mathrm{Acc}} \times \varepsilon_{\mathrm{Rec}} \tag{18}$$

6.5 invariant yield

The π^0 raw yield spectrum (Figure 39) was converted to the invariant yield with efficiency (Figure 40). The π^0 invariant yield in p-Pb collisions at $\sqrt{s_{\mathrm{NN}}} = 5.02$ TeV is shown in Figure 41.

This result does not take account of systematic uncertainties, for example detector uncertainties such as energy resolution, residual mis-calibration, π^0 raw spectrum from the finite accuracy in the invariant mass fitting and other uncertainties. To compare with the previous results in different energy in different colliding particle species and to evaluate the influence of initial condition in collisions, these uncertainties are needed to consider.

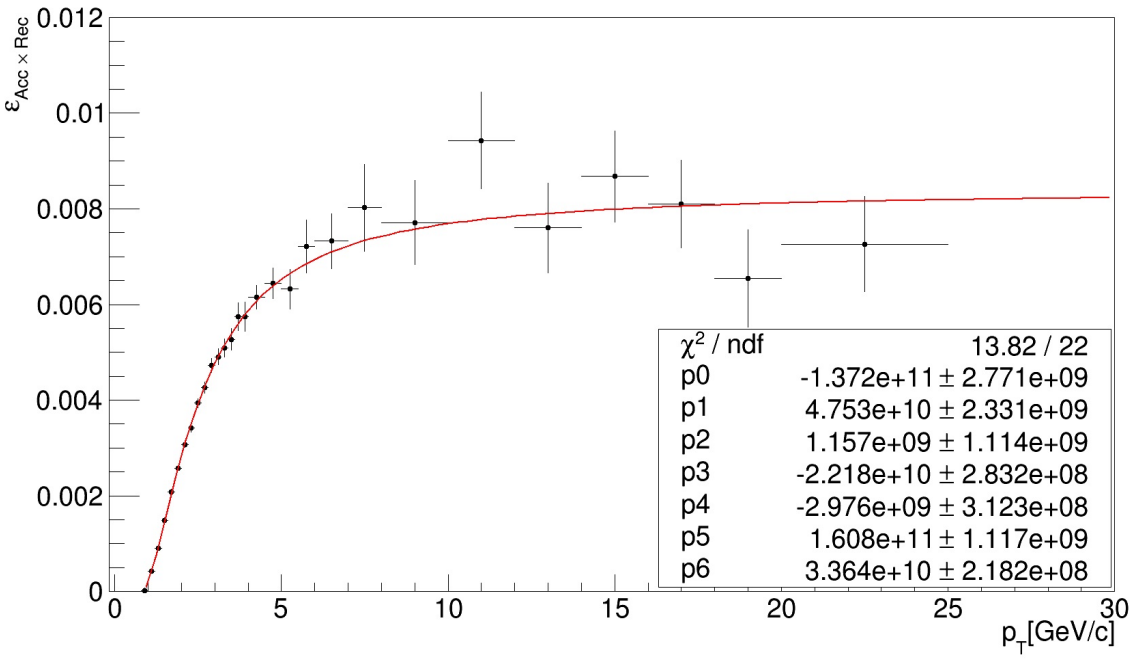

Figure 40: Efficiency

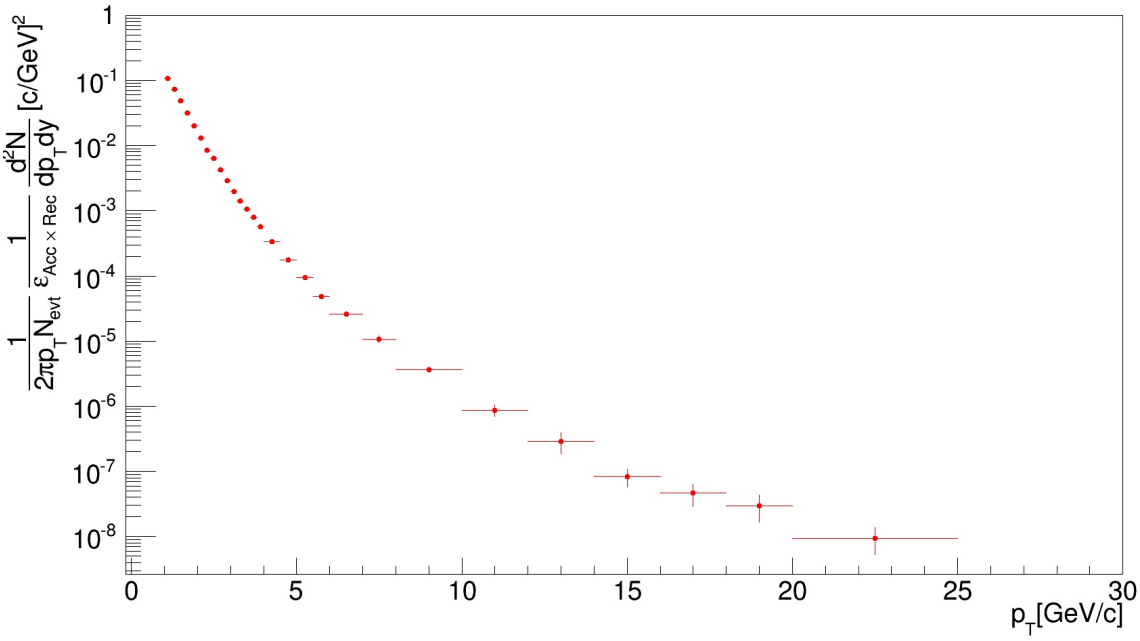

Figure 41: π^0 invariant yield

7 Summary and outlook

We have analyzed PHOS data in p-Pb collisions at $\sqrt{s_{\rm NN}}$ = 5.02 TeV. The analysis used about 8×10^7 minimum bias triggered events. We assessed the data quality to obtain the reliable physical result. In the quality assessment, the good cells were selected by estimation for measured energy and detected the number of particles in each cell in each run. After good runs selection with cluster energy, the number of cells per cluster and the number of clusters per event, we estimated the accuracy of energy measurement in PHOS with the ratio of energy-to-momentum (E/p) for electron. A non-linearity effect in $p_{\rm T}$ <1.6 GeV/c was found and it increases as a function of $p_{\rm T}$. A slight deviation by 2 % from $E/p = 1$ was also found in $p_{\rm T}$ >1.6 GeV/c. The effect and deviation are caused by bremsstrahlung and energy loss in cluster reconstruction. These were systematically investigated and calibrated depending on modules and momentum, and were no longer observed.

We presented the π^0 invariant yield with PHOS in p-Pb collisions at $\sqrt{s_{\rm NN}}$ = 5.02 TeV for the first time. The π^0 invariant yield was obtained by extraction from invariant mass spectra and correction of acceptance and reconstruction efficiency. The π^0 invariant mass spectra were reconstructed via $\pi^0 \rightarrow 2\gamma$ decay channel. However it needs more investigations for systematic uncertainties such as energy resolution, residual mis-calibration, π^0 raw spectrum from the finite accuracy in the invariant mass fitting and other uncertainties. We can only compare with previous results in different energy and to evaluate the influence of initial condition in collisions when these uncertainties are considered.

At present, the LHC accelerator is Long Shutdown(LS1) for the increase in luminosity. With upgrade of LHC accelerator, the plan to upgrade for ALICE detector is in progress. We are improving the timing resolution and the speed of read-out in PHOS. We expect the data after improving the detector performance.

Acknowledgment

First of all, I gratitude for Prof. T.Sugitate who supported and adviced me on physics. By grace of his suggestions, I was able to improved my perspectivr for physics. I would like to express my thank Prof. K.Shigaki who supported further my academic life. I thank Dr. K.Homma who taught me opinions from different view. I would like to appreciate Mr. Y.Nakamiya who adviced me a lot of physical attitude and also supported me technically. Discussion with him was meaningful. I am grateful Mr. S.Yano. He taught me a way of analysis and knowledges for PHOS. Mr. D.Sato, Mr. D.Sekihata and K.Tarunaga who are a member of ALICE/PHOS group in Hiroshima, supported me by discussing in detail about PHOS. Mr. T.Hoshino and Mr. T.Hasebe are in the same room and I talked them physics and friendly chats. In addition, I appreciate all heartfelt supports by the quark laboratory members.

I would like to express my appreciation to PHOS offline analysis group and PWG-GA(Physics Working Group on Gamma and Neutral Pions), in particular Dr. Y.Kharlov and Dr. D.Peressounko. They helped me by the teaching me information of PHOS and analysis methods.

References

[1] FKarsch, PoSCPOD 07, 026 (2007)

[2] T.K.NAYAK, arXiv:1201.4264v1(2012)

[3] F.Karsch, arXiv:hep-lat/106019v2(2001)

[4] S.S.Adler et al. (PHENIX Collaboration), Phys. Rev. Lett. 94, 232301(2005)

[5] BNL PHENIX Home Page, http://www.phenix.bnl.gov/

[6] A. Adare et al. (PHENIX Collaboration), Phys. Rev. Lett. 104, 132301(2010)

[7] L.Evans and P.Bryant(editors), "LHC Machine" 2008 JINST 3 S08001

[8] ATLAS Home Page, http://atlas.ch/

[9] ALICE Home Page, http://aliceinfo.cern.ch

[10] The ALICE collaboration, "The ALICE Experiment at the CERN LHC" 2008 JINST 3 S08002

[11] T.Bird(University of Southampton), "An Overview of the ALICE Experiment"

[12] CERN/LHCC 2003-049, ALICE Physics Performance Report, Volume1 (7 November 2003); The ALICE Collaboration: F.Carminati et al., J.Phys. G:Nucl. Part. Phys. 30(2004) 1517-1763

[13] The ALICE collaboration, "ALICE Technical Design Report of the Computing"

[14] Y.Hori(University of Tokyo), "Mixed harmonic azimuthal corrections in $\sqrt{s_{\rm NN}} = 2.76$ TeV Pb-Pb collicions measured by ALICE at LHC", Doctor thesis

[15] The ALICE Collaboration, The ALICE Offline Bibble

[16] D.Alexandrov et al., "A high resolution electromagnetic calorimeter based on lead-tungstate crystal" Nucl.Instrum.Meth.A550:169-184,2005

[17] B.Abelev et al. (The ALICE Collaboration), Physics Letters B717(2012) 162-172

[18] Y.Maruyama(Hiroshima University), "Development search of PHOS test bench for the ALICE experiment", Master thesis

[19] The ALICE collaboration, "ALICE Technical Design Report of the Photon Spectrometer (PHOS)"

[20] O.Driga et al. (The ALICE collaboration), "Data quality assessment for the ALICE PHOS detector"

[21] J.Midori(Hiroshima University), "Study of neutral mesons with the PHOS triggered data in proton-proton collisions at $\sqrt{s} = 7$ TeV", Master thesis

[22] S.Yano(Hiroshima University), "Analysis of π^0, η and ω mesons in pp collisions with a high energy photon trigger at ALICE", Master thesis

[23] ALICE Combined PID: the ALICE PID framework,
twiki cite "https://twiki.cern.ch/twiki/bin/view/ALICE/PWGPPParticlIdentification"

[24] Y.Iwanaga(Hiroshima Universiy), "Measurement of high p_{T} K^0_S mesons in Au+Au collisions at $\sqrt{s_{\mathrm{NN}}} = 200$ GeV" Master thesis

Appendix : Run list for analysis (LHC13bc)

Run index	Run number	Analyzed events
0	195344	109965
1	195351	447499
2	195389	474796
3	195390	522808
4	195391	721308
5	195478	157511
6	195479	4878868
7	195480	1042773
8	195481	132670
9	195482	1446165
10	195483	9997525
11	195529	0
12	195531	25234967
13	195566	3178690
14	195567	3286538
15	195568	9627642
16	195592	683196
17	195633	5632836
18	195635	1186644
19	195644	6836154
20	195673	4337731
21	195677	1771925